

ELECTRIC FIELD INDUCED ISOTROPIC-NEMATIC PHASE TRANSITIONS IN
NEGATIVELY ANISOTROPIC DISCOTIC LIQUID CRYSTALS

A Thesis

by

UGOCHUKWU DAVID OKEIBUNOR

Submitted to the Office of Graduate and Professional Studies of
Texas A&M University
in partial fulfillment of the requirements for the degree of

MASTER OF SCIENCE

Chair of Committee,
Committee Members,

Zhengdong Cheng
Lei Fang
Micah J. Green

Head of Department,

Arul Jayaraman

May 2020

Major Subject: Chemical Engineering

Copyright 2020 Ugochukwu Okeibunor

ABSTRACT

The nematic phase represents the most fluid liquid crystalline phase. The high shape anisotropy and long range orientational order of constituent particles in this phase yields wide-ranging applications from high strength fibers even to liquid crystal display technology. This wide relevance makes the investigation of the assembly of liquid crystals structures into such ordered domains of paramount importance in soft matter phenomena. External fields have been proposed as a means to effectively control nematic ordering. Discotic liquid crystals, in the presence of external fields, are hypothesized to form a unique, higher-ordered, biaxial nematic phase. Herein, we experimentally demonstrate for the first time, the phase transitions of colloidal nanoplates that possess negative anisotropic polarizability in an electric field. We synthesize α -Zirconium Phosphate nanoplatelets by the hydrothermal method, and these disks are exfoliated in aqueous medium using tetra-(n)-butyl hydroxide to yield very low aspect ratio monolayers. In the absence of any fields, we observe an isotropic-nematic transition as concentration increased. We demonstrated that small cell thicknesses around 120 μm provided clear schlieren textures for the disclinations of the nematic phase. Experiments investigating the phase behavior of these nanoplatelets under the effect of an external electric field yielded results consistent with theoretical extensions of the Onsager theory. The phase diagram in the field strength vs concentration plane reveals the existence of a tricritical point where a second-order transition meets with a first-order phase transition. The first order transition is characterized by coexistence between a uniaxial phase and biaxial nematic phase (characterized by bi-isogyre disclinations). The second order transition is characterized by a direct transition from a paranematic phase to the highly anisotropic biaxial nematic phase. Our

experiments demonstrate that electric fields offer a vital tool to control the self-assembly of nanoplate liquid crystals and could be translated other 2D systems such as graphene oxide by scaling with respect to factors including aspect ratio, polydispersity, anisotropy. Furthermore, the biaxial nematic phase could be useful to 3D imaging technology by wielding the ability to control the alignment of particles along two axes with a unidirectional electric field.

ACKNOWLEDGEMENTS

Much gratitude to the Artie McFerrin Department of Chemical Engineering for the continued support of the student in the completion of this thesis. Without this support, this work would not have been possible.

Many thanks to my adviser and committee chair, Dr. Zhengdong Cheng. Through the past two years you have pushed and driven me to aim and work hard to excel. Much thanks to my lab mates, Abhijeet Shinde, Dali Huang, Mingfeng Chen; you welcomed me into this lab with open arms and helped train me to become proficient in experiments and you were always available and willing to guide me. Much thanks to the department's graduate advisors Ashley and Terah for your continued support and being an added resource. Much thanks to my classmates, especially Marco, George and Jarad for your friendship, and the good times.

Finally much thanks to my family. My uncle and aunt for their undying support for me through the past years. And my mom for your prayers and consistent effort to help me become the most successful man I can be.

CONTRIBUTORS AND FUNDING SOURCES

Contributors

This work was supervised by a thesis committee consisting of Dr. Zhengdong Cheng (chair), Dr. Micah Green of the Department of Chemical Engineering, and Dr. Lei fang of the Department of Chemistry. This thesis was completed by the primary author, with additional support and mentorship from colleagues including Abhijeet Shinde, Dali Huang and Mingfeng Chen, as well as added discussions and collaboration with Dr. Padetha Tin from the NASA Glenn Research center.

Funding Sources

The student was entirely supported by a Research/Teaching Assistantship provided by the Artie Department of Chemical Engineering at Texas A&M University. The research work was supported in part by NASA grant NNX13AQ60G.

NOMENCLATURE

ζ^{-1}	Inverse Aspect Ratio
EBS	Electric Birefringence Spectroscopy
$f(\theta)$	Orientalional Distribution of Particles
I-N	Bi-phasic Region
O	Oxygen
Zr	Zirconium
S	Disclination Strength
SEM	Scanning Electron Microscopy
ITO	Indium Tin Oxide
TBACl	Tetrabutylammonium Chloride
TBAOH	Tetra(<i>n</i> -butyl ammonium) hydroxide
TEM	Transmission Electron Microscopy
V_p	Volume of Particle
g	Grams
μm	Micrometer
mL	Milliliter
$\text{ZrOCl}_2 \cdot \text{H}_2\text{O}$	Zirconyl Chloride Hydrate
ZrP	Zirconium Phosphate
$\Delta\alpha$	Anisotropy of Polarizability
ρ_{water}	Density of Water
ϕ	Volume Fraction
ϕ_{water}	Volume Fraction of Water
ϕ_I	Isotropic threshold concentration

ϕ_N

Nematic threshold concentration

TABLE OF CONTENTS

ABSTRACT.....	iii
ACKNOWLEDGEMENTS.....	v
CONTRIBUTORS AND FUNDING SOURCES.....	vi
NOMENCLATURE.....	vii
TABLE OF CONTENTS.....	ix
LIST OF FIGURES.....	xi
LIST OF TABLES.....	xiv
CHAPTER I: INTRODUCTION.....	1
About Liquid Crystals.....	1
Self-Assembly of Liquid Crystals.....	3
CHAPTER II: FREE ENERGY COMPUTATIONS FOR LIQUID CRYSTAL.....	9
Onsager’s Theory – Effect of Excluded Volume and Entropy.....	9
External Fields Contribution to Free Energy.....	12
CHAPTER III: ZIRCONIUM PHOSPHATE PLATELETS.....	15
Synthesis of α -Zirconium Phosphate Platelets.....	15
Isotropic Nematic Phase Separation.....	21
CHAPTER IV: EXTERNAL FIELD INDUCED ALIGNMENT.....	25
Effects of Cell Thickness on Schlieren Textures.....	25
Electric Field Induced Phase Transitions.....	31
First Order Transitions.....	32
Second Order Transitions.....	41

Phase Diagram.....	44
CHAPTER V: CONCLUSIONS AND FUTURE WORK.....	47
REFERENCES	49

LIST OF FIGURES

Figure		Page
1	Molecular order within isotropic liquid, liquid crystal and crystal materials. Liquid crystals possess an intermediate degree of positional and orientational order.....	1
2	Phase diagram of positive anisotropic (a) and negative anisotropic (b) in the presence of an external field. Both phase diagrams include a biphasic region. The phase diagram of negative anisotropic materials further includes a tricritical point where a first order transition meets a second order transition.....	7
3	Isotropic-Nematic phase transition in calamatic particles. The isotropic phase occurs at low concentrations and lacks any form of order with high orientational entropy. The nematic phase forms at higher concentration and favors translational entropy.....	11
4	Onsager-Parsons phase diagram for discotic liquid crystals. With increasing concentrations (volume fraction), the isotropic phase evolves into a nematic and then a columnar phase. Very high aspect ratios are required to form the nematic phase.....	12
5	Coordinate system definition for Zirconium Phosphate disks with electric field application. The direction of the electric field is constant; parallel to the z-axis. The direction of the particle director is specified by polar angle θ and azimuthal angle.....	14
6	ZrP discs in (a) granular form and (b) powdery form. The powdery form is exfoliated into solution	16
7	Scanning Electron Microscopy Image a) 5kV, b) 10kV of ZrP platelets synthesized by hydrothermal method.....	18

8	Exfoliation of Zirconium Phosphate Platelets. The multi-layer structure is separated into thin anisotropic monolayers by tetra-butyl ammonium hydroxide.....	19
9	Exfoliated Zirconium Phosphate nanoplatelets in solution with water and tetra(n-butyl ammonium) hydroxide. The solution appears cloudy as a result of high concentration of platelets.....	19
10	The initial preparation of Zirconium Phosphate Liquid Crystal Suspensions with volume fraction from 0.006 to 0.012. The nematic domains are brightly colored.....	21
11	The I-N phase separation 6 hours after sample preparation for volume fraction from 0.006 to 0.012. The crystals are clearly observed in solution and sedimentation / phase separation commences.....	22
12	The I-N phase separation achieved days after sample preparation for volume fraction from 0.006 to 0.012. The nematic phase, composed of higher fraction of platelets sediments to the bottom of the vial. The less-dense isotropic phase stays on top.....	23
13	Phase Diagram plot for ZrP nanoparticles. The nematic fraction increases as a function of volume fraction of platelets.....	24
14	Schematic for Electric field Experimentation. The sample is contained within a spacer sandwiched between ITO glass plates. The voltage generator provides an electric field to induce alignment.....	25
15	Schlieren textures with full and half integer strengths. Full integer ($s=1$) disclinations possess four dark brushes/isogyres around it while half integer defects have two dark isogyres.....	27
16	Polarized Microscopy Image of 50% Nematic Sample with spacer thickness a) 120 microns b) 240 microns c) 360 microns. No electric field is applied.....	28

17	Polarized microscopy image of 50% nematic Sample with spacer thickness and electric field voltage: a) 120 μm , 3V b) 240 μm , 6V c) 360 μm , 9V. Increasing cell thickness / sample volume leads to distortion.....	29
18	Schematic for experimentation to determine transition points for ZrP platelets in electric field. The first order transition occurs in sufficiently highly concentration of platelets whilst the second order transition occurs in very low concentrations.....	32
19	Schematic for experimentation to determine first order transition points for ZrP platelets in volume fraction ranges within the electric field.	33
20	Nematic Phase formation for $\phi = 0.008 \pm 0.001$ at applied voltages 0.0V to 10.0V. The sample thickness was constant at 120 μm . The para-nematic region is characterized by increase in brightness of the domains. The transition from the para-nematic into the biphasic region is characterized by crystal formation.....	34
21	First Order Transition Voltage Extrapolation $\phi = 0.008 \pm 0.001$. The transition voltage is defined as 2.5V (0.0208V/ μm). This represents the transition from the paranematic to the biphasic region.....	35
22	Schematic for experimentation to determine first order transition points for ZrP platelets in volume fraction ranges within the electric field..	36
23	Schlieren Texture of particles at 0V to 1.5V for volume fraction $\phi = 0.012 \pm 0.001$. Application of the electric field induces brightening as well as a uniaxial-biaxial transition. The uniaxial defects are characterized by four dark brushes while the biaxial defects are characterized by two dark brushes.....	38
24	First Order Transition Voltage Extrapolation for volume fraction $\phi = 0.012 \pm 0.001$. The transition voltage is defined as 1.4V (0.0117V/ μm). This represents the transition from the coexistence to the biaxial region.....	39
25	Defect Splitting in the Nematic Phase for $\phi = 0.011 \pm 0.001$ with applied voltage of 2.5V _{pp} . The biaxial nematic phase is featured with two dark brushes, which are formed by the splitting of four dark brushes.....	41

26	Schematic for experimentation to determine second order transition points for ZrP platelets in volume fraction ranges within the electric field.....	42
27	Microscopic enlargement of particles at voltages 250V, b) 300V, c) 300V for $\phi = 0.0032 \pm 0.0002$. Application of electric field below this concentration leads to a second order transition to the biaxial phase.....	43
28	Phase diagram of ZrP Particles in Electric Field. The 1 st order transition occurs from the para-nematic phase to the biaxial phase, The 2 nd order transition occurs from a co-existence phase to the biaxial phase.....	45

LIST OF TABLES

Table		Page
1	Classification of liquid crystals. Liquid crystals can be classified by shape, property and phase.....	2
2	Summary of effect of cell thickness on the schlieren textures observed in polarized microscopy imaging. Higher cell thickness leads to denser defects and indiscernible features.....	30
3	Transition voltages for first order transitions below I-N coexistence volume fractions. The transition point decreases roughly linearly with volume fraction..	36
4	Transition voltages for first order transitions within I-N coexistence volume fractions. The transition point decreases roughly linearly with volume fraction..	40
5	Transition voltages for samples within volume fraction. The transition point decreases exponentially with volume fraction.....	45

CHAPTER I: INTRODUCTION ¹

About Liquid Crystals

Liquid crystals represent a characteristic state of matter with properties between that of a solid crystal and an isotropic liquid. In the traditional crystal state, constituent molecules possess a defined long-range positional order as well as orientational order. In the traditional isotropic state, molecules lack both long-range positional and orientational order, resulting in fluid properties. The liquid crystal state possesses unique orientational and positional ordering of the molecules, in between that of a liquid. Figure 1 below demonstrates the varying levels of ordering in liquids, liquid crystals and crystals.

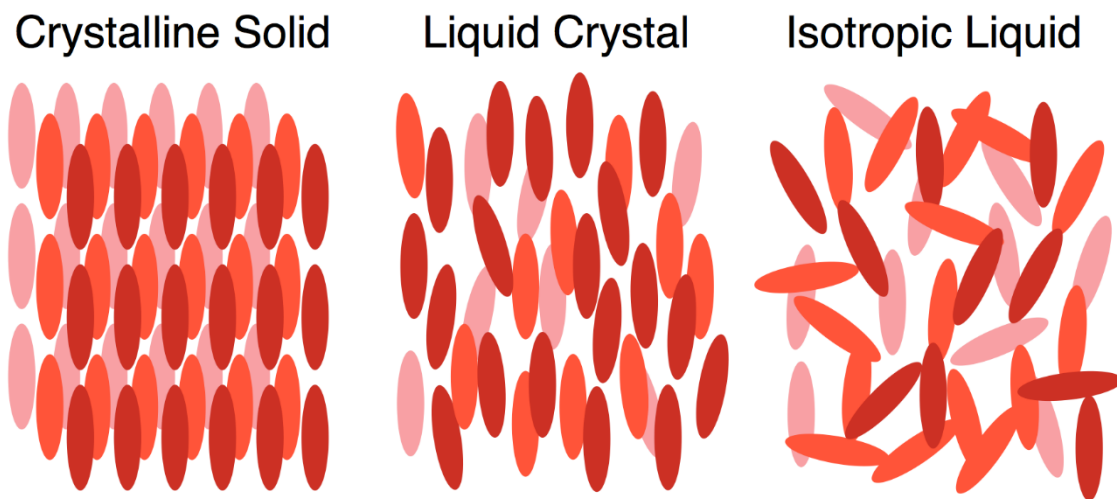


Figure 1. Molecular order within isotropic liquid, liquid crystal and crystal materials. Liquid crystals possess an intermediate degree of positional and orientational order.⁷¹

¹ Parts of this chapter is reprinted with permission from “External Field Induced Tricritical Phenomenon in the Isotropic...” by Varga et al, Year. *Molecular Physics*, Vol. 98, 911-915, Copyright 2020 by Taylor & Francis Online.

Liquid crystals were originally identified by botanical physiologist Friedrich Reinitzer in 1888, when he was examining various derivatives of cholesterol, which had been previously identified to exhibit colorful effects at temperatures slightly above the freezing point.²⁴ Reinitzer discovered that cholesteryl benzoate melted in two phases, first from a solid to a cloudy liquid, and then from the cloudy liquid to a clear liquid. His work was followed up by Otto Lehman who reported the existence of crystallites within the structure; these crystallites, were responsible for the unique phase behavior. Lehman discovered the ability of these substances to affect the polarization of light, flow like a liquid, and at the same time these substances possessed crystal-like order. Thus these materials were termed “liquid crystal”.²⁴

Through decades of research, since the original discovery of liquid crystals, hundreds of molecules and materials have been found to yield liquid crystal behavior in a variety of phases and structures.^{25, 51-56} The table below summarizes the classification of liquid crystals.






Shape	Property	Phase
 Discotic	Thermotropic	 Nematic 
 Calamatic		Lyotropic
 Bent-core		

Table 1. Classification of liquid crystals. Liquid crystals can be classified by shape, property and phase.^{32,37}

Liquid crystals can be classified based on shape – discotic, calamitic or bent cores.⁵⁰ These different geometries possess, in common, a high degree of shape anisotropy; this is responsible for their ability to organize into some form of order unlike the isotropic phase. Liquid crystals can also be classified based on behavior; lyotropic liquid crystals attain some level of order and by increased concentration of the particles within solution, however, the phase behavior of thermotropic liquid crystals depends on temperature.⁵⁷ Finally, liquid crystals can be classified by phases. The simplest liquid crystal phase is the nematic phase, which possesses long-range orientational order but no positional order. The smectic phase possesses long-range orientational order as well as 1D positional order. The columnar phase possesses long-range orientational order and 2D positional order.

Since their discovery, liquid crystals have yielded a wide range of applications including drug delivery,^{28,29} liquid crystal lenses, medical thermography, high strength fibers,³⁰ spectroscopy, and most importantly the ‘liquid crystal display’ technology.^{23,32} This usefulness makes the exploration of liquid crystalline alignment behavior of paramount importance.

Self-Assembly of Liquid Crystals

The self-assembly and phase transitions of liquid crystals has been in the limelight of active research due to its importance and translation in traditional display technology and other areas.¹ It is well known that the mesophase transition behavior of liquid crystals is a result of subtle balances between the state of entropy of the particles,² and thus is strongly dependent

on intrinsic particle properties such as geometry.³ Work conducted thus far has identified three major geometries of liquid crystals - discotic, calamitic and bent-core shapes, each with unique phase behaviour.⁴ In particular, the calamitic and discotic geometries of liquid crystals have been very important in soft matter phenomena due to their ability to form a distinct nematic phase with increasing concentration.⁵ The nematic phase, as a result of its high degree of translational entropy, represents the most fluid state a liquid crystal can attain, and investigation of colloidal systems that can align into such structure is thus paramount in soft matter applications.⁵⁻⁶

Some of the earliest and most widely acclaimed works on the isotropic-nematic (I-N) transition in hard convex bodies was performed by Onsager. Onsager, very importantly, demonstrated that the formation of the nematic phase can be attributed to the hard-body interactions between particles to maximize entropy and minimize free energy.⁷ Onsager modeled the I-N transition as a minimization of the free energy of particles using trial functions up to the second virial coefficient. More recent work since Onsager's such as Parsons have included higher virial coefficients to adequately describe the phase transitions in particles of finite, shorter geometries.

External fields have been identified to yield a means to adequately control the assembly of liquid crystals molecules. Three sources of external fields - electric fields, magnetic fields^{40,45} and flow fields³⁸ - have displayed the ability to re-orient / re-align particles within a phase and furthermore, to induce crystal phase transitions.¹¹ Past investigations, including work by Khokhlov and Semenov have corroborated the fact that all external field types yield

qualitatively identical effects on the isotropic-nematic transition in colloidal crystals-
minimization of a biphasic region until attainment of a critical point.^{7,12}

The very ability of calamitics and discotics to form a nematic phase in the presence of an electric field has been attributed to the high anisotropy of these geometries. The anisotropy of electric polarizability, represented as $\Delta\alpha = \alpha^{\parallel} - \alpha^{\perp}$ is the difference in polarizability parallel to the main axis of the particles and perpendicular to the main axis.⁷ In the absence of fields, particles typically have their normal directed randomly across the whole domain. However, upon application of an external fields, particles tend to develop orientational order with their normal either perpendicular or parallel to the field. In the case where the normal of particles is more inclined parallel to the field, particles exhibit positive anisotropy, and vice versa. Discotics have been shown to be more prone to a negative polarizability anisotropy due to a stronger polarization across the longer axis.⁷ Rod-like systems on the other hand, are more prone to display positive anisotropy of polarizability. This mere difference in orientation around a field directly predicts the phase behavior attained. Varga et al showed that while the phase behavior of platelets, with negative polarizability yielded the convergence of a first order and second order transition, rod-like systems with positive anisotropy yielded only a first order transition.¹

In the case of negative polarizability, using simulation and theoretical modelling, Varga et al demonstrated the existence of a tricritical point at the point of convergence between a second and a first order transition.⁷ Each phase can be characterized based on polarized microscope imaging. When observed under a polarized microscopy system, the isotropic state lacks any birefringence, the paranematic phase displays birefringence, schlieren textures of the uniaxial phase are particularly characterized by $s = 1$ defects with four dark brushes, while those

of the biaxial phase is characterized by $s = \frac{1}{2}$ defects, with two dark brushes.¹⁴ These defects of the nematic phases simply represent discontinuities in local orientation.

The ability to induce the alignment of liquid crystals using external fields has thus been of paramount importance; by such means, we are able to control the dynamics of and also to yield unique mesophase behaviors. Previous work by Chen et al investigated the behavior of Zirconium Phosphate suspensions in the presence of a magnetic field and found discotic liquid crystals to align their normal parallel to a magnetic field, displaying positive diamagnetic susceptibilities and thus forming wholesome superstructure domains.¹⁵

Discotic molecules provide a highly anisotropic shape with a rich phase behavior,⁶¹ yet their properties are not well identified compared to the calamatic molecules. Previous works on the assembly of disks have been largely focused on theoretical simulations with very limited experimental work.⁵⁸ The discotic systems due to high anisotropy shapes form the uniaxial nematic phase.⁵⁹ In the absence of an external field, the biaxial nematic phase is elusive for discotic systems.⁶⁰ Van den Pol et al showed that while the uniaxial nematic phase was formed as a result of increasing concentration, only particles with roughly equivalent length-width and width-thickness ratios could form a distinct biaxial nematic phase⁸, possessing high degree of orientational order along two axes.⁹⁻¹⁰

Previous works have focused on deducing the phase diagram using simulation models based off trial functions extended from Onsager's theory. Khoklov and Semenov demonstrated a major difference between the mesophase behaviour arising as a result of interactions of positive anisotropic dielectric particles versus negative anisotropic dielectric particles. Whereas

both displayed a minimization in a biphasic region with increasing field strength, a characteristic tricritical point was observed to occur as a result of interactions within the negatively anisotropic particles, at which point a second order and first order transition coincided. Figure 2 below demonstrates the difference in phase behavior for positive anisotropic and negatively anisotropic materials.

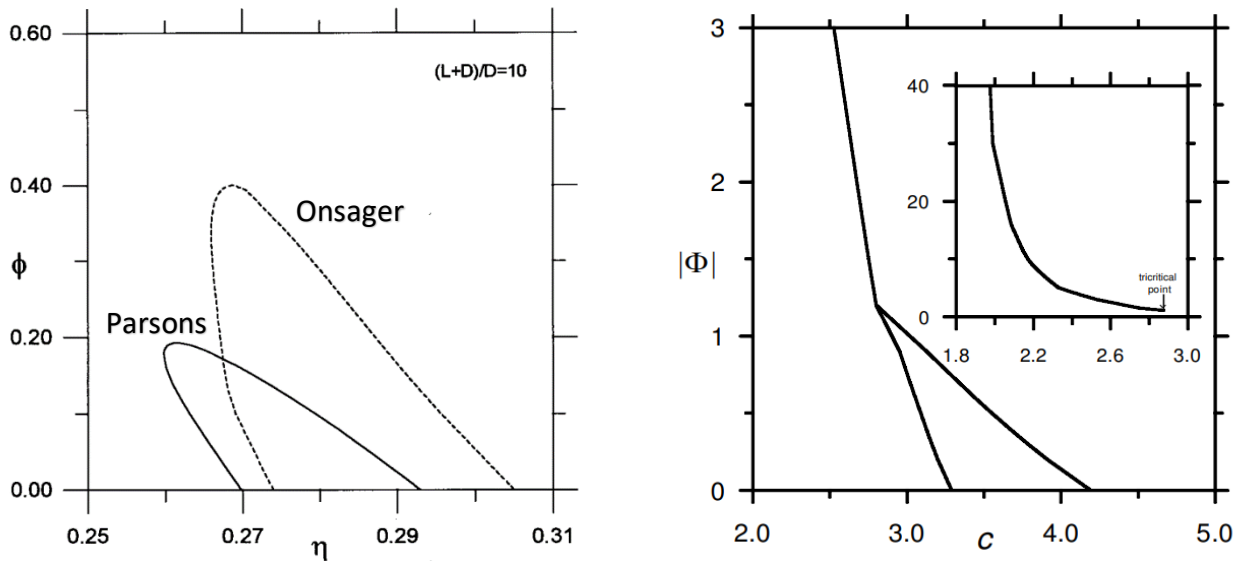


Figure 2. Phase diagram of positive anisotropic¹² (a) and negative anisotropic⁷² (b) in the presence of an external field. Both phase diagrams include a biphasic region. The phase diagram of negative anisotropic materials further includes a tricritical point where a first order transition meets a second order transition.

The phase transition behavior of discotic nanoparticles has not been thoroughly identified and investigated in literature. In this present study, we investigate, experimentally, the comprehensive phase behavior, comprising a first order uniaxial-biaxial transition, of discotic liquid crystals with negative anisotropic polarizability in an electric field. We aim to derive this phase behavior in a field strength-concentration plane using Zirconium Phosphate suspensions. The deduced phase diagram is posited to include the existence of a tricritical point

at which a second order transition and a first order transition converge, in line with Onsager and Parsons approximation for hard-convex bodies with negative anisotropy. The major implication for this work is deeper understanding of phase behavior and biaxiality in colloidal suspensions. The biaxial phase represents an extremely fluid, higher order liquid crystalline phase and this attribute poses great potential for faster switching in liquid crystal display technology,⁴⁷ than the traditional uniaxial phase currently employed. Furthermore, by gaining a better understanding of relationship between electric field intensity and nematic phase dynamics/defects, we can mitigate the problem of non-uniformities and contrast incoherence in Liquid Crystal Displays.

CHAPTER II: FREE ENERGY COMPUTATIONS FOR LIQUID CRYSTALS ²

Onsager Theory- Effects of Entropy and Excluded Volume on Free Energy

Some of the earliest work on the isotropic-nematic transition of liquid crystal systems was performed by Onsager. Onsager appropriately identified that high aspect ratios of molecules resulted in shape anisotropy and thus, the ability to form a liquid crystal nematic phase. He observed that in a system of sphero-cylindrical/rod-like molecules, as the concentration of the particles increased, the particles aligned to a preferred direction.

Onsager proposed that the arrangement of these particles was driven by the attempt to maximize free volume of each particle; thus, although orientational entropy was lost, translational (packing) entropy was gained in the Isotropic to nematic phase transition. Onsager defined an orientational distribution function³⁵ which could adequately define the orientational order of a given particle³⁶:

$$f(\omega) = \frac{\alpha \cosh(\alpha \cos \theta)}{4\pi \sinh \alpha}$$

Where ω is an orientational unit vector defining the direction of the particle and specified by the azimuthal angle (φ) and polar angle (θ), α represents a varying parameter whose value is obtained by minimizing the free energy, $f(\omega)$ defines the probability of a particle being at an orientation ω , and is normalized:

$$\int f(\omega) d\omega = 1$$

² Parts of this chapter is reprinted with permission from "Aspect Ratio and Polydispersity Dependence of Isotropic-Nematic...." by Meija et al, 2012, Phys Rev E., Vol. 85, Copyright 2020 by American Physical Society.

In the isotropic phase, all directions are equally probably and thus $f(\omega)$ is constant ($\frac{1}{4\pi}$); in the nematic phase, there is a favored long range directional order, and $f(\omega)$ varies. Using this trial function, Onsager defined the free energy of rods in a liquid crystal suspension. Therein, the free energy of a hard convex body (F_{hcb}) is directly related to an orientational entropy term $\sigma[f]$ and a packing entropy term, $\rho[f]$. Onsager defined both of these terms:

$$\sigma[f] = \int f(\omega) \ln(4\pi f(\omega)) d\omega$$

$$\rho[f] = \frac{4}{\pi} \int |\sin(\gamma(\omega_1\omega_2))| f(\omega_1)f(\omega_2) d\omega_1 d\omega_2$$

Using the virial coefficient up until the second term for density computations (which is accurate for very high aspect ratios, as in the case of our system), Onsager derived the energy functional for the hard convex body:

$$\frac{F_{hcb}[f]}{NkT} = \ln(c) - 1 + \sigma[f] + c\rho[f]$$

Where k represents the Boltzmann constant = $1.38 \times 10^{-23} \text{m}^2 \text{kg s}^{-2} \text{K}^{-1}$, T is the temperature, N is the number of molecules⁷⁰, and c represents the concentration defined for a discotic system as:

$$c = \frac{\pi^2 D^3 N}{16V}$$

Here, D represents the diameter of the particle, N represents the number of particles, V represents the volume of particle. This equation can be simplified by incorporating the definition for the volume fraction $\phi = \frac{NV_p}{V}$, and aspect ratio $\zeta = \frac{L}{D}$. The volume of the particle

$V_p = \frac{\pi D^2 h}{4}$ is related to the total volume, V . Therefore, the reduced concentration can be expressed as

$$c = \frac{\phi \pi D}{4h} = \frac{\pi \phi}{4\zeta}$$

Onsager's theory yields a qualitative method to understand the formation of a liquid crystal nematic phase. The formation of the liquid crystalline phase is governed by a minimization of the excluded volume of each particle and subsequent gain in translational entropy. In the isotropic phase, the particles are randomly distributed with no long range order; the orientational entropy is maximized. However, as the particle concentration increases, there is a need to achieve a more efficient packing and this is attained by orienting along a specific direction. While such packing minimizes the orientational entropy, the excluded volume is reduced, thus allowing for more free volume and a higher degree of translational entropy. Figure 3 below demonstrates the isotropic to nematic phase transition.



Figure 3. Isotropic-Nematic phase transition in calamitic particles. The isotropic phase occurs at low concentrations and lacks any form of order with high orientational entropy. The nematic phase forms at higher concentration and favors translational entropy.

At even higher concentrations, many more structured liquid crystal phases are observed to occur with higher degree of order than the nematic phase as a result of interparticle

interactions. Phase diagrams have been constructed as a function of increasing concentration and even for varying aspect ratios of particles. Figure 4 demonstrates the phase behavior of disks based on their aspect ratio; low aspect ratios are required to form the distinct nematic phase, but at very high concentrations the particles assume long range positional order in the columnar phase.

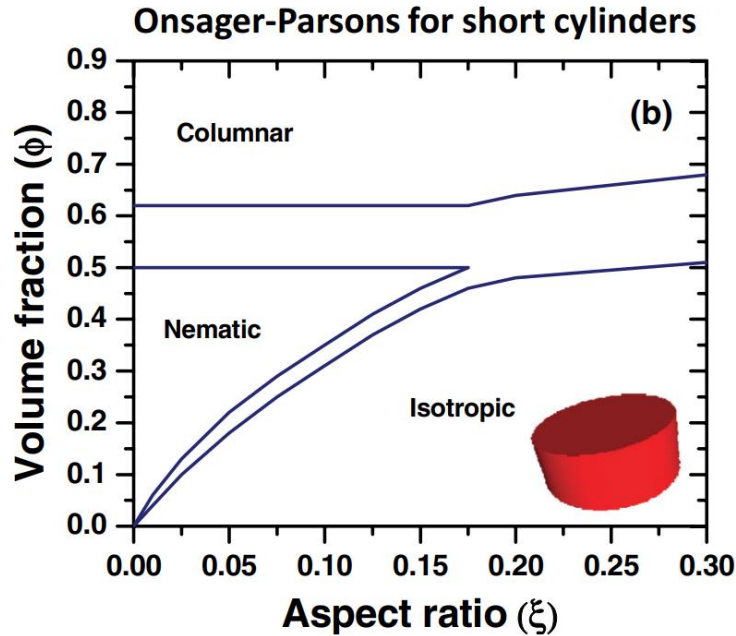


Figure 4. Onsager-Parsons phase diagram for discotic liquid crystals. With increasing concentrations (volume fraction), the isotropic phase evolves into a nematic and then a columnar phase. Very high aspect ratios are required to form the nematic phase.²⁰

External Fields Contribution to Free Energy

In our discussions so far, we have neglected the influence of external fields and focused on phase behavior as a sole result of inter-particle interactions. Accounting for the influence of external stimuli/fields on overall particle interactions, the total free energy functional of hard convex bodies becomes a sum of the field independent (F_{hcb}) and field dependent (F_{ext}) terms.²

$$\frac{F[f]}{NkT} = \frac{F_{hcb}[f]}{NkT} + \frac{F_{ext}[f]}{NkT}$$

The field independent term is defined already and depends on factors such as concentration and orientation of the platelets. The influence of the external fields on the free energy functional is independent of field direction and defined in relation to a field strength parameter (Φ) as¹³:

$$\frac{F_{ext}[f]}{NkT} = -\Phi \int f(w) \cos^2(\psi) d\omega$$

Here, ψ represents the angular difference between the director of a particle and the direction of the field and Φ represents the electric field parameter, defined for an electric field as follows:

$$\Phi = \frac{(\alpha^{\parallel} - \alpha^{\perp})E^2}{4kT} = \frac{\Delta\alpha E^2}{4kT}$$

Where $\Delta\alpha$ represents the anisotropy difference of the particles between the main axis of the particle and the respective perpendicular axis, E represents the electric field strength - defined as the voltage V across a distance, k represents the Boltzmann constant = $1.38 \times 10^{-23} \text{m}^2 \text{kg s}^{-2} \text{K}^{-1}$ and T is the temperature.

In the case of our system, we employ the traditional definition of Cartesian axes – x , y and z , as well as the angular definitions within spherical coordinates (θ , φ). The electric field is generated in a vertical direction by a positive and negative electrode each connected to conductive ITO glass plates. Let us define φ_{Φ} and θ_{Φ} as specifying the orientation of the

nematic field. We limit the direction of electric field direction in the positive z-direction with no dependence on the azimuthal angle therefore $\varphi_\phi = \theta_\phi = 0$.

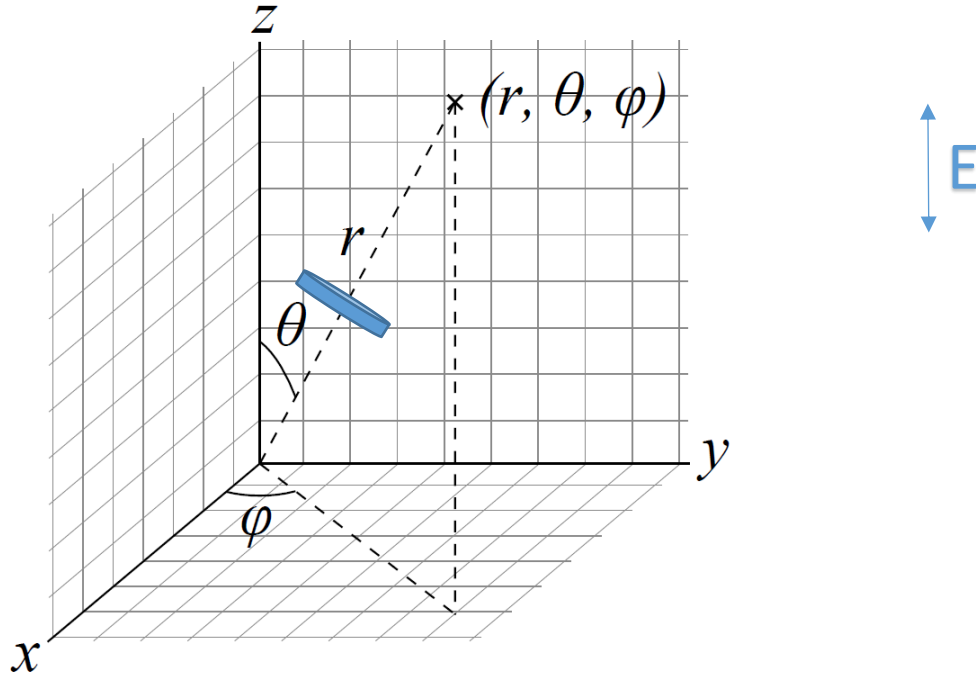


Figure 5. Coordinate system definition for Zirconium Phosphate disks with electric field application. The direction of the electric field is constant; parallel to the z-axis. The direction of the particle director is specified by polar angle θ and azimuthal angle φ .

The function $\cos(\psi)$, can be defined as a scalar product of the electric field direction (ω_ϕ) and the nematic director (ω).⁷² We thus expand the external field contribution to the free energy as:

$$\frac{F_{ext}[f]}{NkT} = -\Phi \int \int f(\theta, \varphi) \{ \sin(\theta_\phi) \sin(\theta) \cos(\varphi_\phi - \varphi) + \cos(\theta_\phi) \cos(\theta) \}^2 \sin(\theta) d\theta d\varphi$$

For $\theta_\phi = 0$ then:

$$\frac{F_{ext}[f]}{NkT} = -\Phi \int \int f \cos^2 \theta \sin(\theta) d\theta d\varphi$$

CHAPTER III: α -ZIRCONIUM PHOSPHATE NANOPATELETS

Synthesis of α -ZrP Nanoplatelets

The formation of liquid crystal phase requires a distinct high anisotropy shape. Liquid crystal phases have been known to form from a variety of molecular shapes all characterized as composing of distinct rigid structures which enable the formation of highly anisotropic phases. The colloidal liquid crystal materials used in this study were suspensions of α -Zirconium Phosphate (ZrP) nanoparticles. The unique structure of synthetic ZrP nanomaterials has found general applications in Pickering emulsions, coatings, functional membranes, and even drug delivery systems. The layered structure of Zirconium Phosphate was elucidated by Clearfield in 1968 as consisting of a octahedral network of Zr, P and O atoms of length 6.6Å with interlayer water molecules of thickness 1Å [B]. The synthesis of ZrP disks was well documented by Yu [C]; ZrP discs can be synthesized by three major methods- hydrothermal, reflux and microwave assisted.

For the purpose of this study, ZrP discs were synthesized by the hydrothermal method in a two-step process. Compared to the other methods of synthesis, the hydrothermal method yields very high aspect ratios for the particle and thus higher anisotropy. The first step in synthesis was hydrothermal production of pristine ZrP disks. This was achieved by combining 6g of zirconyl chloride octahydrate ($ZrOCl_2 \cdot H_2O$, 98+%, Acros organics) with 60 ml of 15M phosphoric acid (85%, Fisher Scientific). This mixture was stirred, placed in a PTFE container within an autoclave and then set in an oven (Fisher Scientific) at 200 °C to be treated for a duration of 6 hours. The reaction occurred as described below:



This formation of liquid crystalline order within the ZrP disks occurs in two steps. The first stage is the nucleation of crystals and the second stage is crystal growth. Upon completion of the reaction, the solution was obtained and allowed to cool to room temperature. The solution was mixed and thoroughly and separated into four 50ml centrifuge tubes. These tubes were placed into a centrifuge machine (Thermo Scientific; CL-2) and run for 10 minutes at 4000 revolutions per minute. After centrifugation, the sediment particles (ZrP disks) were separated from the less dense solution, water was added and the centrifugation procedure was repeated thrice. Upon the last round of centrifugation, the sediment particles were collected and placed in an oven at low temperature for drying to yield pristine nanoplatelets of zirconium phosphate. Figure 6 shows the particles before and after drying. These grains (6a) were grounded into fine powder (6b) using a mortar and pestle.

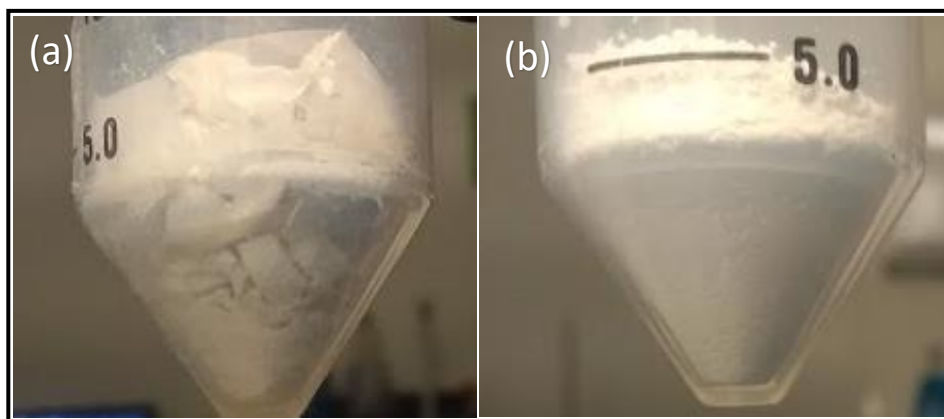


Figure 6. ZrP discs in (a) granular form and (b) powdery form. The powdery form is exfoliated into solution.

The resulting powder mixture of ZrP disks was dissolved in water and characterized by Scanning Electron Microscopy (JEOL JSM-7500F). SEM analysis yielded useful information on the morphology of the disks with respect to geometry and size distribution. A few grams of ZrP powder was dissolved in 7.8 mL of Milli-Q water for 24 hours and also sonicated (VWR-50T) in water for 30 minutes to ensure maximum particle solubility. Figure 7 indicates the solution with water. The discs were further diluted to lower concentration and prepared in a substrate for SEM analysis. Figures indicate discotic geometry for the disks. The average diameter of the ZrP disks measured was 863 nm with a polydispersity greater than 29%. Assuming a ZrP thickness of 2.68 nm, the average aspect ratio of the particles is around 0.0025.

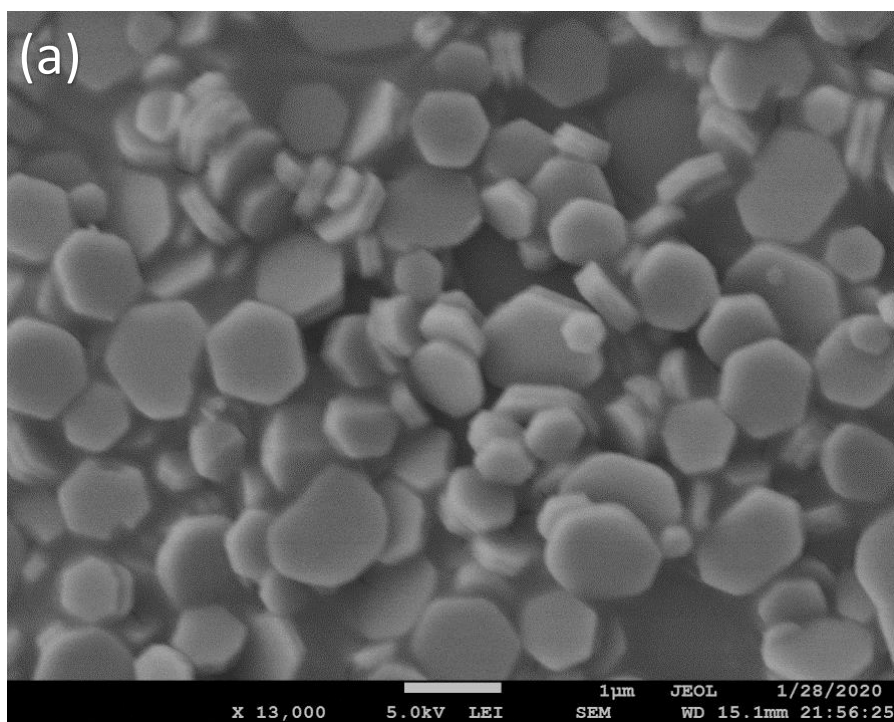


Figure 7. Scanning Electron Microscopy Image a) 5kV, b) 10kV of ZrP platelets synthesized by hydrothermal method

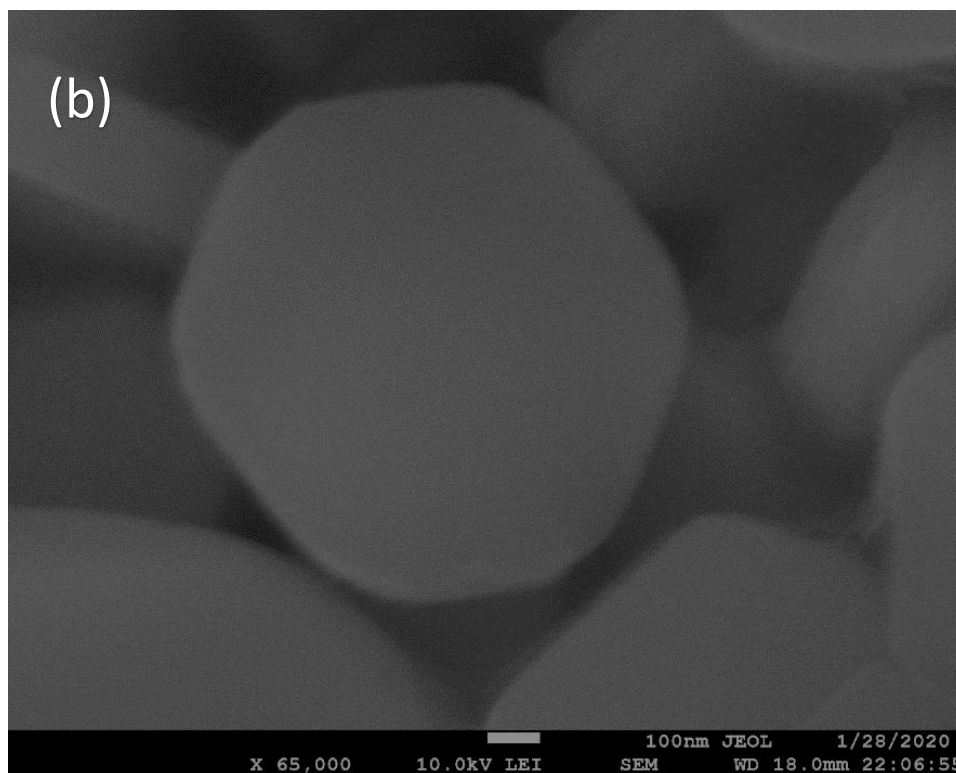


Figure 7. Continued

The second step in synthesis was exfoliation of the pristine disks with tetra-(n) butyl ammonium hydroxide to yield the mother suspension. This was performed by adding small drops of 2.2mL of tetrabutyl ammonium hydroxide solution to the solution whilst stirring using a mini vortex (Fisher Scientific). The reaction is summarized as below:

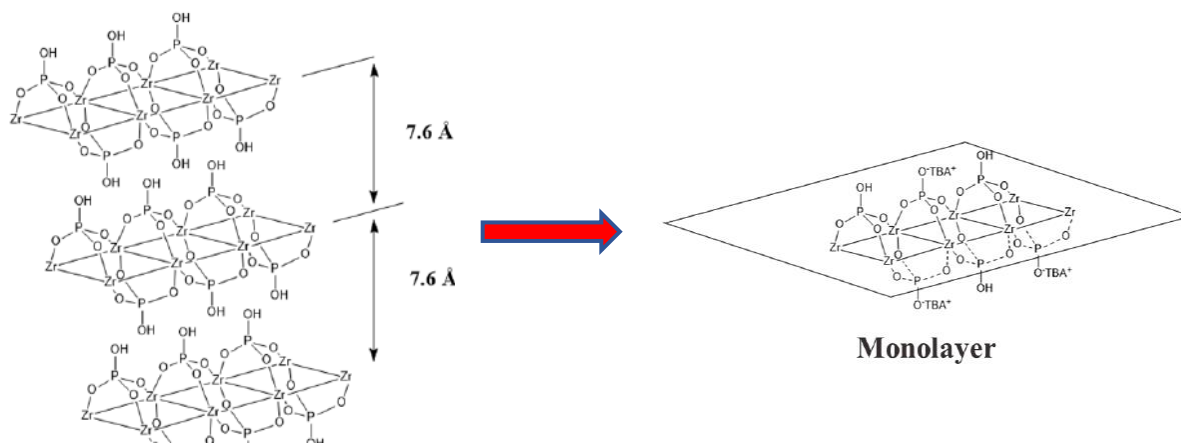
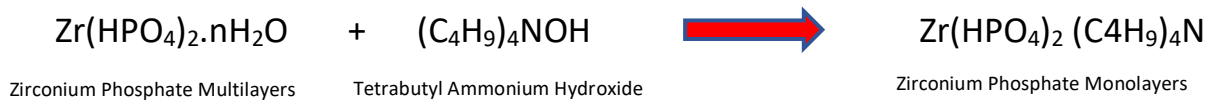


Figure 8. Exfoliation of Zirconium Phosphate Platelets. The multi-layer structure is separated into thin anisotropic monolayers by tetra-butyl ammonium hydroxide.³⁷

Following exfoliation of the particles, the resulting solution is cloudy as demonstrated in figure 9 below.

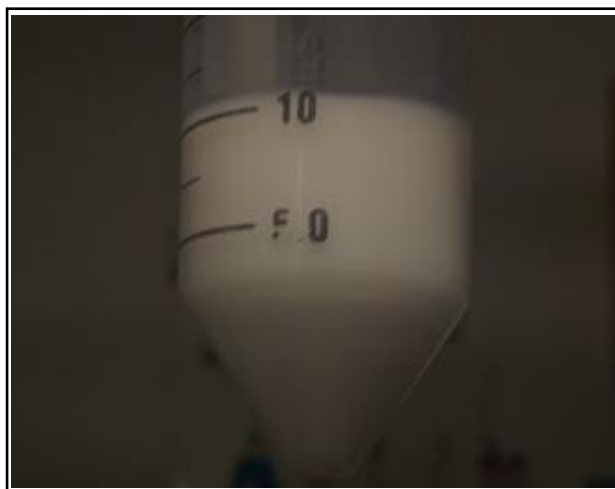


Figure 9. Exfoliated Zirconium Phosphate nanoplatelets in solution with water and tetra(n-butyl ammonium) hydroxide. The solution appears cloudy as a result of high concentration of platelets.

This solution is the mother suspension and the volume fraction was analyzed by collecting 0.40 ml, measuring the mass, and placing in an oven at 65°F, until complete drying of the solvent had occurred. Thus the volume fraction could be calculated by the equation below:

$$\phi_{ZrP} = \frac{0.4mL - \frac{m_i - m_f}{\rho_{water}}}{0.4mL}$$

Where m_i represents the initial total mass, m_f represents the final total mass, the difference of both of which corresponds to the mass of solvent removed by heating, and ρ_{water} is the density of water used to approximate the density of the solvent mostly comprising water. The resulting volume fraction (ϕ) for the mother suspension was 0.059. This represents that the Zirconium Phosphate platelets occupied 5.9% of the total volume within the solution.

Isotropic-Nematic Phase Separation

Gravimetric analysis on the mother suspension yielded a volume fraction of 0.059. This concentration was very high resulting in a very cloudy solution without much display of the characteristic birefringence in liquid crystal nematic phase. This suspension was further diluted to yield samples of concentration range within the isotropic-nematic phase; specifically volume fractions from 0.006 to 0.015. 1ml of each concentration was prepared and poured into a vial; the solvent used was Milli-Q water. Upon preparation, the samples were homogenized using a mini-vortex and set vertically. The percentage nematic fraction was observed between cross polarizers and measurements were made on Image J. Figure10 below depicts the samples right after preparation. Nucleation occurs and nematic domains are characterized by distinct coloration.

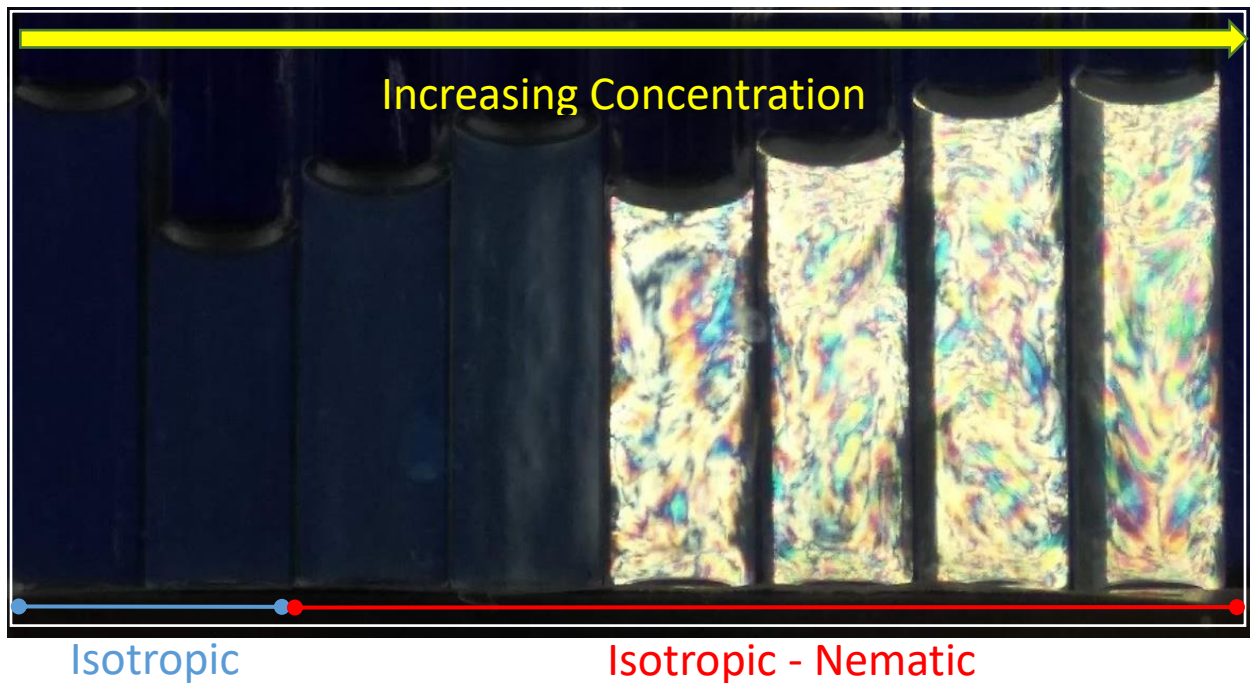


Figure 10. The initial preparation of Zirconium Phosphate Liquid Crystal Suspensions in 1mL vials. Volume fraction ranges from 0.006 to 0.012. The nematic domains are brightly colored.

It was observed that the nematic phase formation was almost instantaneous in higher concentrations which contained enough disks to induce the alignment of the particle directors. The samples were allowed to settle and pictures were taken periodically over two hour intervals. Further imaging of the sample observed that characteristic “wavy” texture observed initially evolved into a texture in which for high enough concentrated vials, the crystal tactoids could clearly be seen in solution. The density of crystals in each vial increased with downward height. Figure 11 below demonstrates images of the vials 6 hours after preparation.

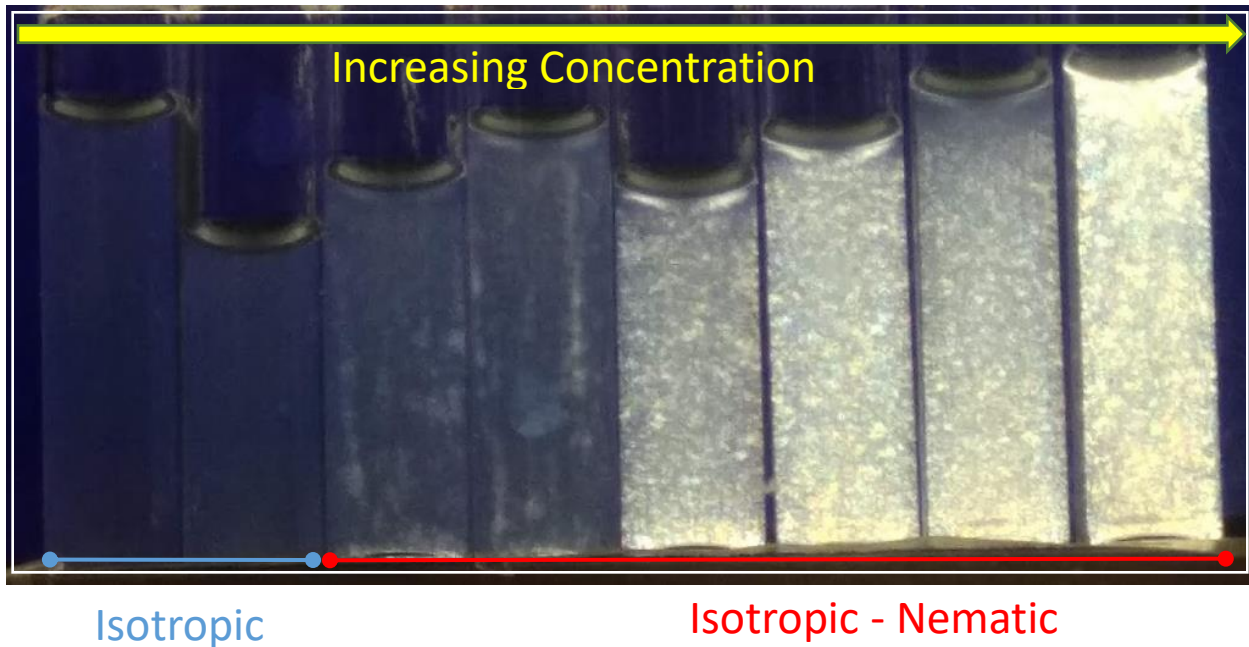


Figure 11. The I-N phase separation 6 hours after sample preparation for volume fraction from 0.006 to 0.012. The crystals are clearly observed in solution and sedimentation / phase separation commences.

Further imaging of the crystal demonstrated a gravity-driven phase separation process in which the crystals began to sediment and isotropic and nematic phases became distinct. For concentrations within the Isotropic-Nematic coexistence phase, the isotropic phase, containing less packing of discotic nanoparticles, remained on top, whereas the more-dense nematic phase settled to the bottom of the vial. The isotropic-nematic phase separation is presents in the figure below.

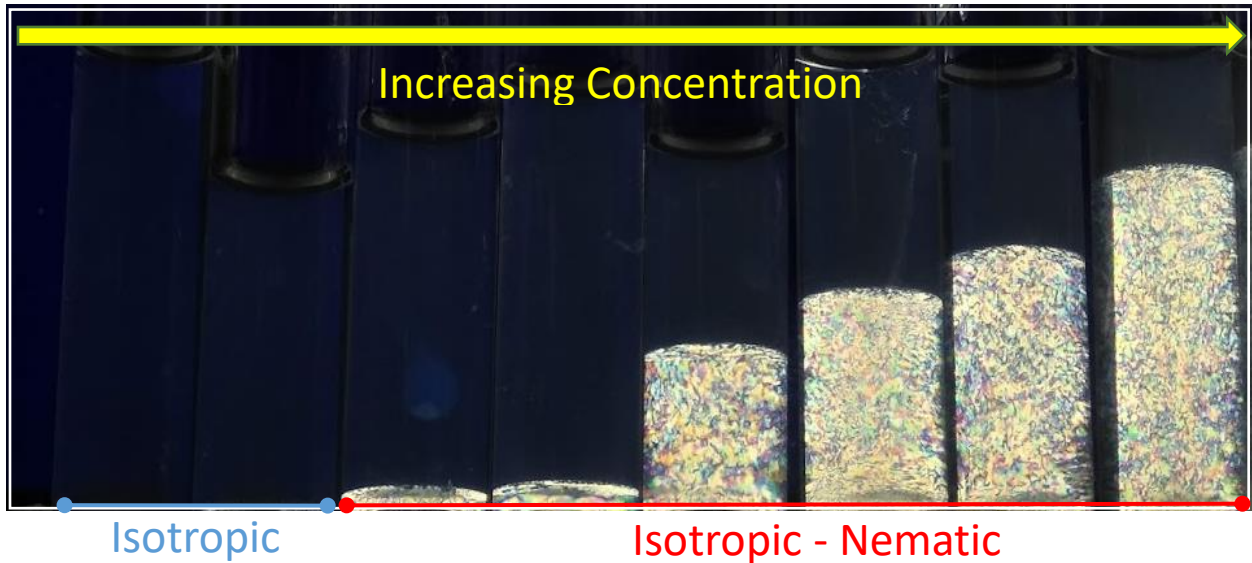


Figure 12. The I-N phase separation achieved days after sample preparation for volume fraction from 0.006 to 0.012. The nematic phase, composed of higher fraction of platelets sediments to the bottom of the vial. The less-dense isotropic phase stays on top.

The nematic height fraction is directly correlated to the % of nematic content of the solution. A phase diagram was constructed to demonstrate the relationship between volume fraction and nematic content. A plot of the % nematic–volume fraction plane was constructed as shown in Figure 13 below; a linear extrapolation was performed for volume fractions within the Isotropic-Nematic coexistence region. This yields an isotropic volume fraction, $\phi_I = 0.0088 \pm 0.0004$, and a nematic volume fraction, $\phi_N = 0.0132 \pm 0.0007$.

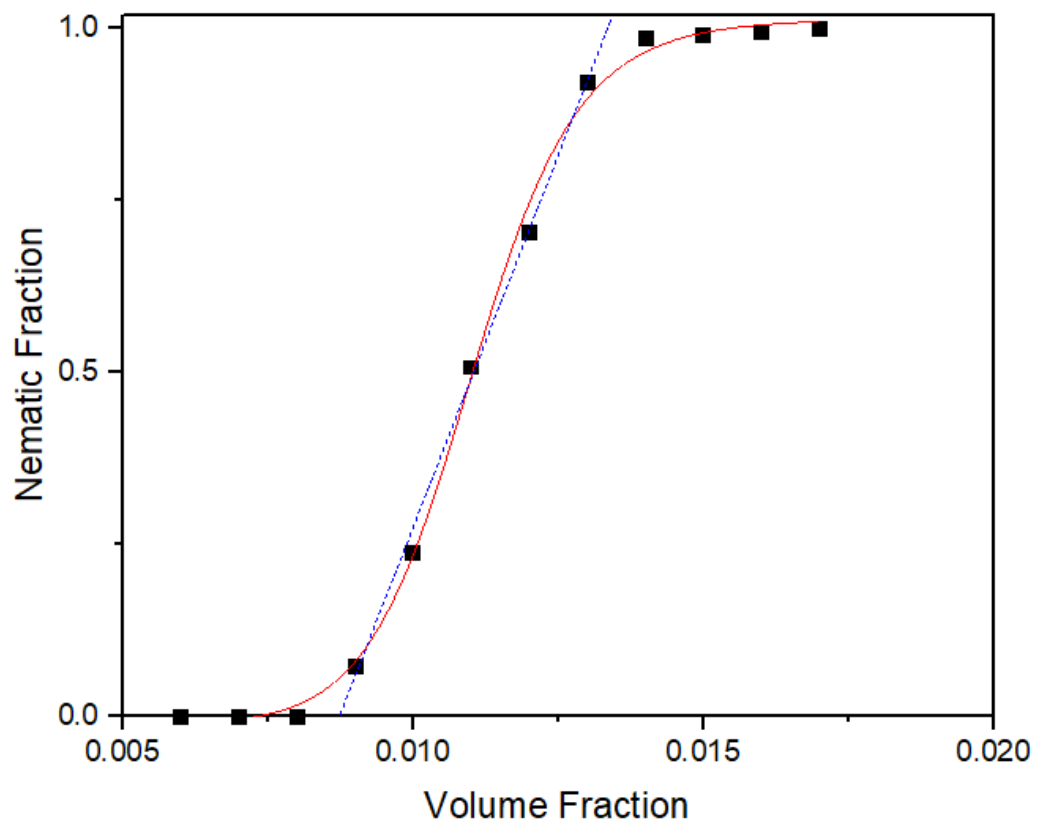


Figure 13. Phase Diagram plot for ZrP nanoparticles. The nematic fraction increases as a function of volume fraction of platelets. The blue line represents a linear extrapolation to yield the 100% isotropic fraction $\phi_i = 0.0088 \pm 0.0004$ and the 100% nematic fraction $\phi_N = 0.0132 \pm 0.0007$.

CHAPTER IV: ELECTRIC FIELD INDUCED TRANSITIONS IN LIQUID CRYSTALS

Effect of Cell thickness on Schlieren Textures

Polarized optical microscopy was employed to observe schlieren textures in the presence of an electric field. The electric field is generated through two electrodes connected to a voltage generator (SRS DS345) which is coupled to a 1000x voltage amplifier (TREK 609-E6) to attain higher electric field strengths. Field direction was specified in the upward z-axis, and independent of the azimuthal angle (φ) to ensure simplification of the system. The electrodes are connected to a pair of Indium Tin Oxide (ITO) glass-plates with the conducting surfaces separated by one or more spacers, each with thickness of 120 microns and inner diameter of 6.35mm. The figure below is a schematic of the set up for the electric field experimentation.

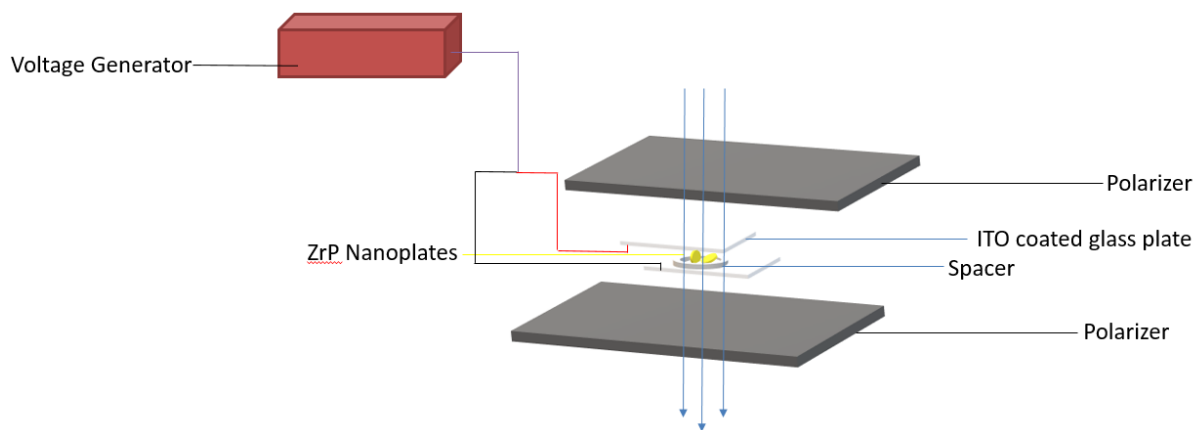


Figure 14. Schematic for Electric field Experimentation. The sample is contained within a spacer sandwiched between ITO glass plates. The voltage generator provides an electric field to induce alignment.

The direction of the light propagation from the microscope is in the z-direction. This was chosen as such based on the discotic geometry of our particles. It is well known that schlieren textures are not observable for light propagation parallel to the optical axis of a particle,

because the optical axis does not exhibit birefringence. For discotic ZrP platelets, as the nematic intensity increases, the optical axis of each particle tends to attain an angle separation of 90° to the direction of the light propagation. This angle enables optimum brightness and observation of the tactoids.

Schlieren textures are an effective means to identify of liquid crystal structures between cross polarizers. These textures are composed of discontinuities in the local directors of particles. In the absence of any orientational ordering, the director of the particles are randomly oriented and thus the polarized image remains dark. However when the molecules have some form of orientational order, the textures are observed to become brighter and form regions of discontinuity in orientational order. The disclinations present in schlieren textures are characterized by their strength “s”. This s-value quantifies the number of rotations the director makes on a full turn around each disclination line;³³ the values range from $\frac{1}{2}, 1, \frac{3}{2} \dots$ For half integral values, the director rotates by odd multiples of π and for full integral values the director rotates by even multiples of π . Generally, lower values of the strength are more stable.³⁴ Figure 15 below is an example of a schlieren texture observed in a polarized microscopy. The positive disclinations rotate in the same direction as rotated polarizers while negative disclinations rotate in the opposite direction as rotated polarizers.^{44,46}

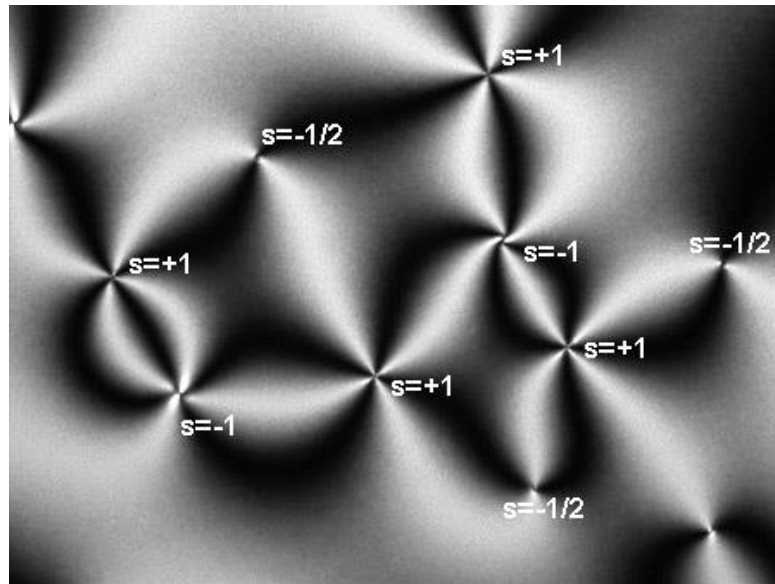


Figure 15. Schlieren textures with full and half integer strengths. Full integer ($s=1$) disclinations possess four dark brushes/isogyres around it while half integer defects have two dark isogyres.³³

We investigated the effect of spacer thickness on the schlieren textures formed within polarized microscope view, and the effect on electric field alignment. For each sample investigated, about 5.0 - 15.0 μ l of fluid with volume fraction $\phi = 0.010$ was loaded within the spacer(s) mounted on an ITO coated glass. This concentration is in the I-N coexistence range with about 50% nematic fraction. Three sets of experiments were run with spacer thicknesses of 120 μ m, 240 μ m, and 360 μ m. After sample loading, an additional ITO coated glass plate was used to sandwich the solution and this was mounted on a microscope stage.

The schlieren textures in the absence of an electric field were observed (figure 16), as well as after the application of field (figure 17).

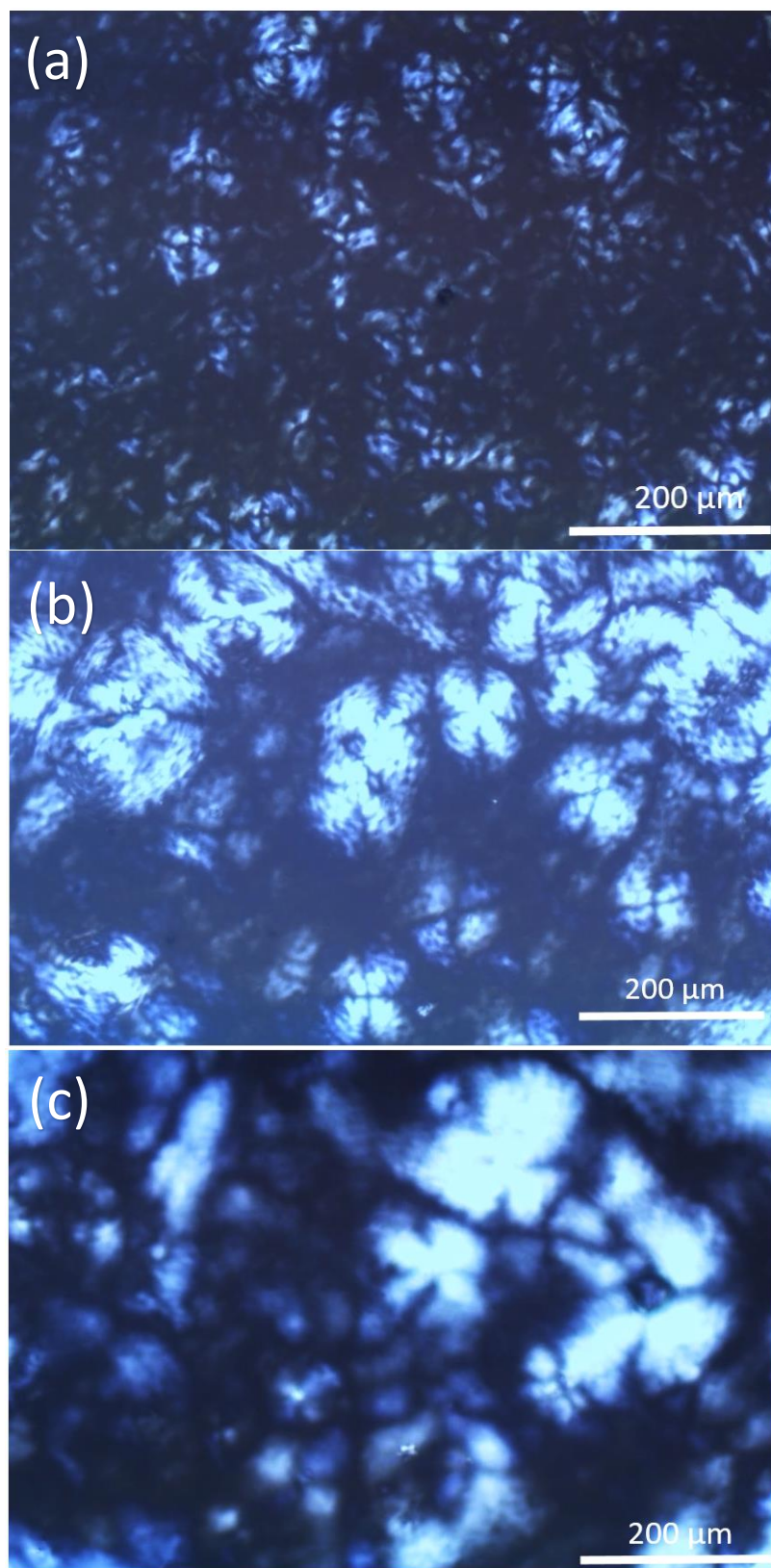


Figure 16. Polarized Microscopy Image of 50% Nematic Sample with spacer thickness a) 120 microns b) 240 microns c) 360 microns. No electric field is applied

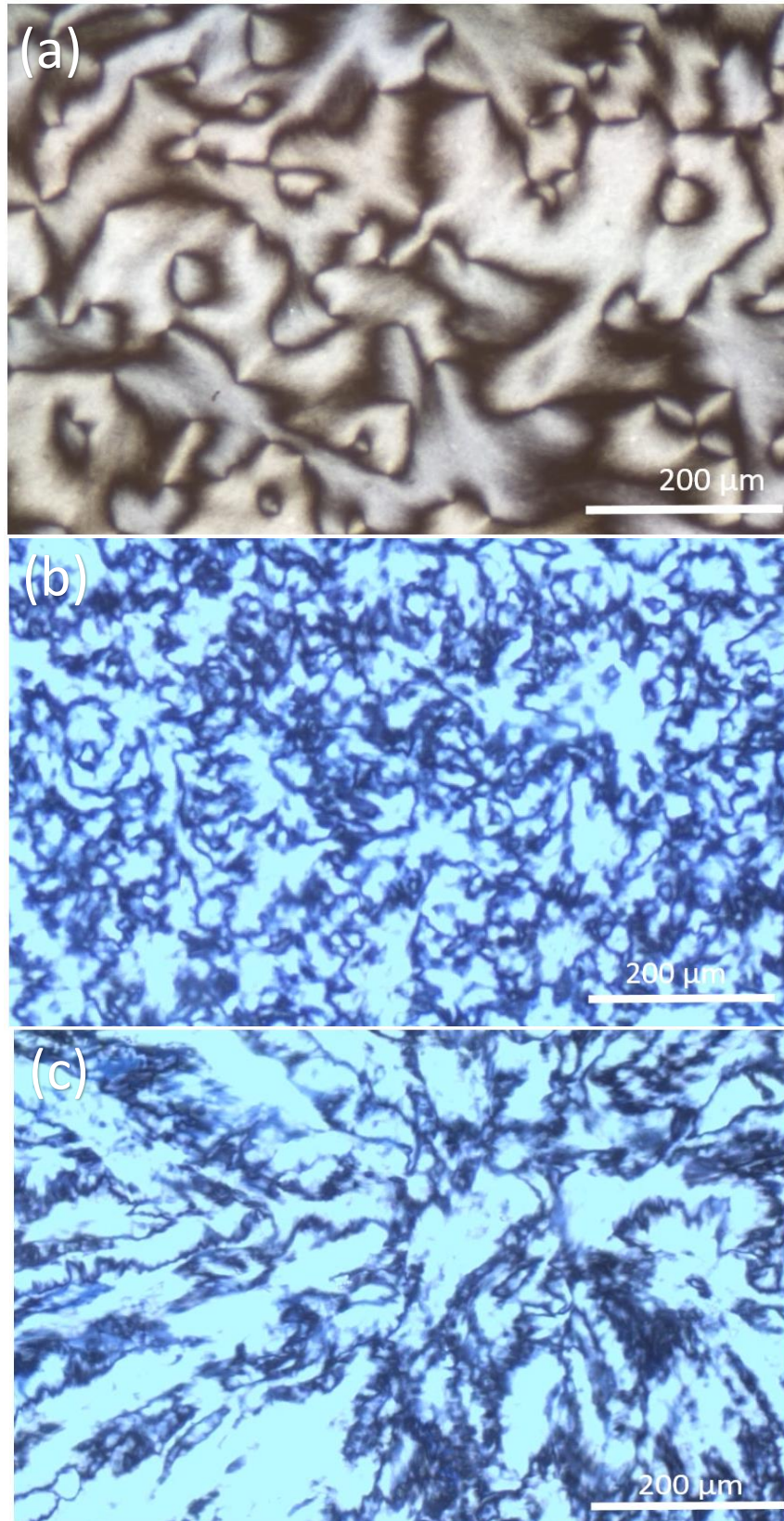


Figure 17. Polarized microscopy image of 50% nematic Sample with spacer thickness and electric field voltage: a) 120 μm , 3V b) 240 μm , 6V c) 360 μm , 9V. Increasing cell thickness / sample volume leads to distortion.

For all cell thicknesses, in the absence of field, the textures indicate the characteristic uniaxial defects (with four dark brushes), coexisting with the isotropic phase. However, larger cell thicknesses resulted in less sharp textures. In the presence of an electric field, the uniaxial phase transitioned to the biaxial phase. The table below summarizes the effects observed

Thickness	Texture Characteristics
120 μm	Clear defects
240 μm	Distorted defects
360 μm	Distorted defects

Table 2. Summary of effect of cell thickness on the schlieren textures observed in polarized microscopy imaging. Higher cell thickness leads to denser defects and indiscernable features.

Electric Field Induced Transitions in Liquid Crystals

A major aim of this study was to experimentally deduce the phase behavior of negative anisotropic ZrP platelets in an electric field. Previous works have predicted that with the application of field, there exists a biphasic region with increasing field strength. This biphasic region concludes at a characteristic tricritical point. This tricritical point represents a point of convergence between a second order and first order transition. These first order transition is characterized by a discontinuity in the order parameter of the phases and exhibits the characteristics of crystal nucleation and growth. The second order transition is spontaneous and has a continuity in the order parameter of the phases.

Experiments conducted were focused on identifying the nature of the first order and second order transition as well as defining the field parameters needed to achieve such transitions. For all experiments, the sample was loaded in to a spacer sandwiched between ITO glass plates and the field was increased slowly. Experiments were conducted at least in triplicate. Trials on the first order transition included volume fractions slightly lower than the isotropic concentration ϕ_I and volume fractions within the I-N coexistence concentrations ($\phi_I < \phi < \phi_N$) from these two sets of data, the tricritical point could be roughly estimated by a linear regression model. Thereafter, the second order transition was investigated by conducting trials at volume fractions lower than the tricritical concentration. Below is a schematic of the experimental design.

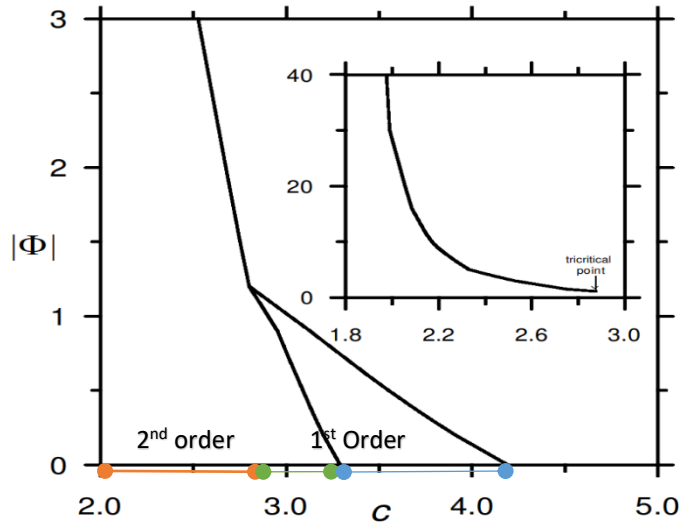


Figure 18. Schematic for experimentation to determine transition points for ZrP platelets in electric field. The first order transition occurs in sufficiently highly concentration of platelets whilst the second order transition occurs in very low concentrations.

First Order Transition

Nematic phase formation ($\phi_c < \phi < \phi_I$)

At concentrations slightly below the concentration of the isotropic phase ϕ_I , but higher than the tri-critical concentration ϕ_c , as the field strength increases, a first order transition commences, initially characterized by nucleation and formation of crystals. In this range of volume fractions, the concentrations of ZrP platelets is not high enough to induce some form or orientational entropy and thus the system exists in an isotropic state. The first order transition occurring here represents a discontinuous change in the state of order as a result of a shift from the isotropic phase to a nematic phase.²³

Based on extrapolation of the physical phase diagram, the value of the isotropic concentration ϕ_I is 0.088. The electric field was applied to samples with volume fraction less

than ϕ_I , specifically $\phi = 0.06, 0.07$ and 0.08 . Below is a schematic of the experimentation. Each sample at a particular concentration was loaded and the electric field was gradually increased.

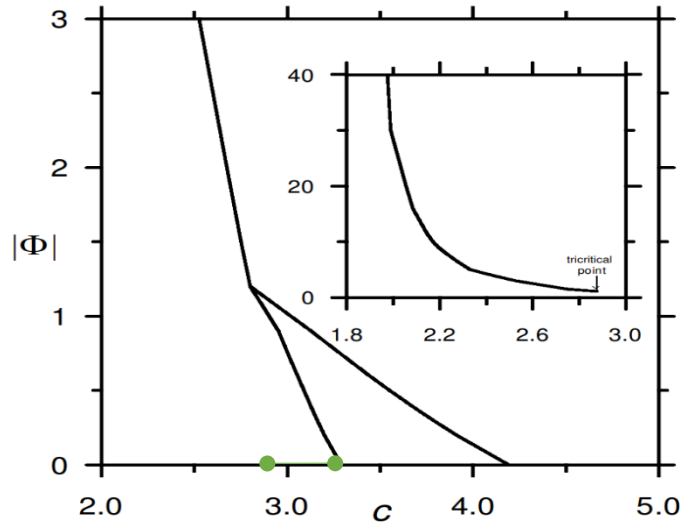


Figure 19. Schematic for experimentation to determine first order transition points for ZrP platelets in volume fraction ranges ($\phi_C < \phi < \phi_I$) within the electric field.

Upon the application of electric field, the sample is observed within a cross polarized microscopy system. It is observed that initially there is a brightening of the domains within polarized microscopic observation; this is explained as a rotation of the director of the particles along the. This phase is defined as the para-nematic phase – the particles are developing some form of order however not high enough to the extent of the nematic phase thus crystal domains are not observed. As the field strength is increased, and the particles obtain higher orientational order, this increase in brightness, gradually progresses to the formation of crystals. Polarized images are for $\phi = 0.0080$ are displayed in figure 20 below. The domains become brighter at first and then the crystal formation begins to occur.

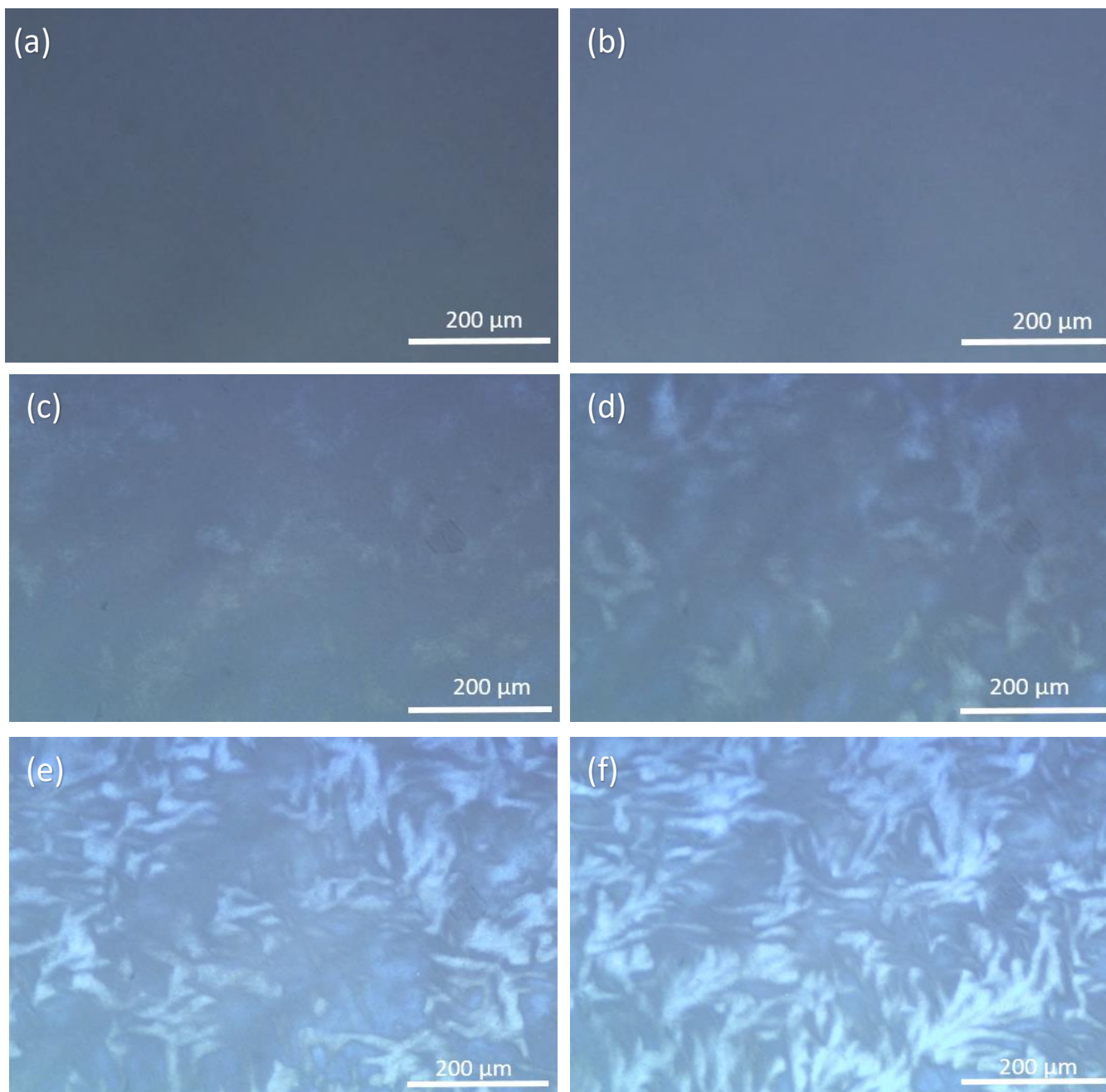


Figure 20. Schlieren textures for $\phi = 0.008 \pm 0.001$ at applied voltages a) 0.0V, b) 1.0V, c) 3.75V, d) 5.0V, e) 7.5V, f) 10.0V. The sample thickness was constant at 120μm. The paranematic region is characterized by increase in brightness of the domains. The transition from the para-nematic into the biphasic region is characterized by liquid crystal formation.

The transition point to be defined is that from the para-nematic phase to the biphasic region. This point is defined as the initial formation of crystal domains. To define this point, the polarized images in figure 20 were characterized using Gwyddion Visual Analysis Software (2019). Factors considered were brightness of the domains as well as density of crystals. A linear extrapolation, as in figure 21 below, was made to the point of 0% and this yielded an applied voltage of 2.5V. This is defined as the transition point for volume fraction $\phi = 0.0080$.

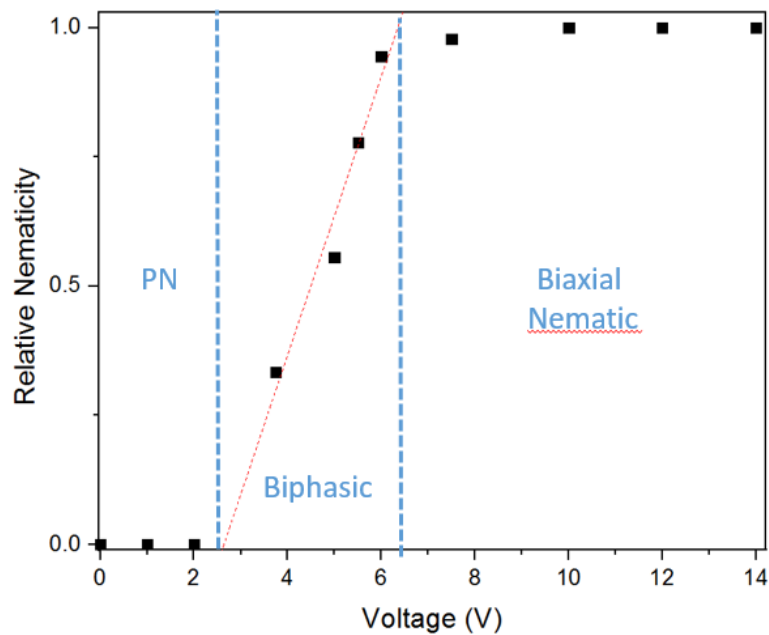


Figure 21. First Order Transition Voltage Extrapolation $\phi = 0.008 \pm 0.001$. The transition voltage is defined as 2.5V (0.0208V/ μm). This represents the transition from the paranematic to the biphasic region.

This procedure was repeated for volume fractions of 0.0060 and 0.0070 to yield transition voltages of approximately 7.0V and 4.0V. The table below summarizes the transition voltages for the set of experiments within concentration range ($\phi_c < \phi < \phi_l$)

Volume Fraction (ϕ)	Transition Voltage (V)
0.006	7.0 ± 0.7
0.007	4.5 ± 0.5
0.008	2.5 ± 0.3

Table 3. Transition voltages for samples within volume fraction ($\phi_c < \phi < \phi_I$). The transition point decreases roughly linearly with volume fraction.

Uniaxial-Biaxial Splitting ($\phi_I < \phi < \phi_N$)

The electric field was applied for ranges of concentration of particles within the uniaxial-biaxial coexistence region $0.0088 < \phi < 0.0132$. This was done to observe the crystal alignment in the coexistence phase as well as the first order uniaxial-biaxial transition. The method of experimentation is demonstrated below. For each concentration, the field is increased slowly.

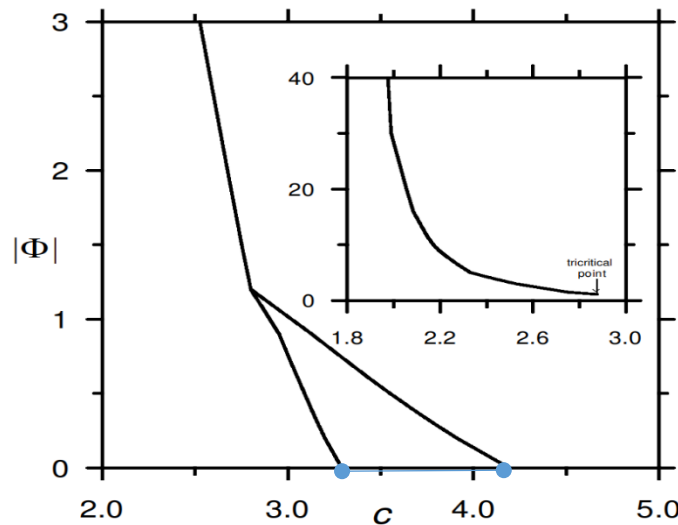


Figure 22. Schematic for experimentation to determine first order transition points for ZrP platelets in volume fraction ranges ($\phi_I < \phi < \phi_N$) within the electric field.

Schlieren are provided below for samples with volume fraction $\phi = 0.012$, equivalent to a nematic fraction of 70%. In the absence of an external field, these samples form a uniaxial-

isotropic coexistence phase. The texture of the polarized image is very dark and comprised of the characteristic 4-isogyre disclinations for the uniaxial nematic phase as well as the characteristic dark texture for the isotropic phase. Once the field is applied, the domain becomes very visibly brighter as a result of alignment of the particle directors. This increase in brightness is coupled with defects splitting. The texture becomes decreasingly uniaxial with the splitting of uniaxial defects ($s = 1$) into biaxial defects ($s = \frac{1}{2}$). Polarized images are for $\phi = 0.011$ are displayed in figure 23 below.

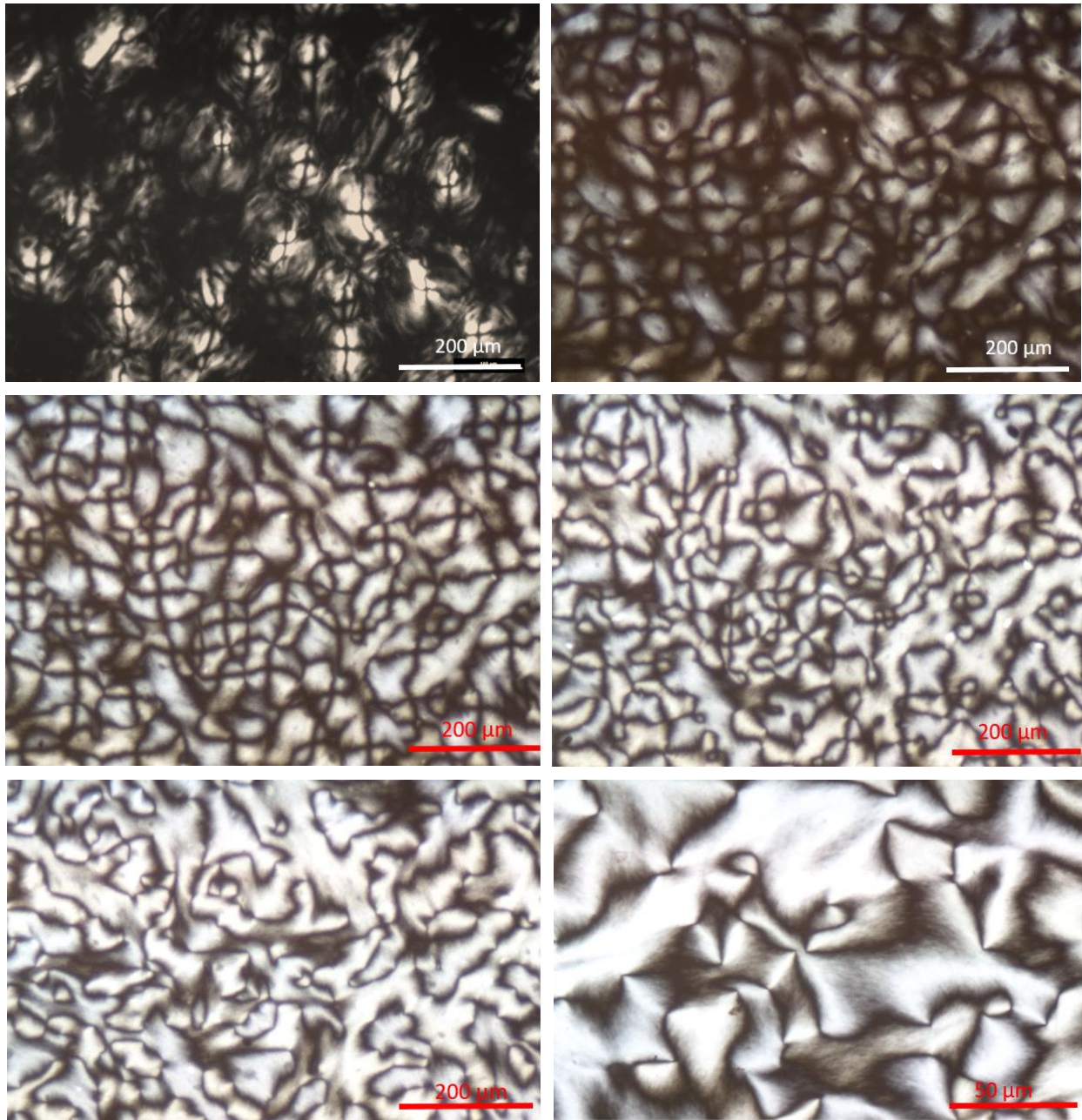
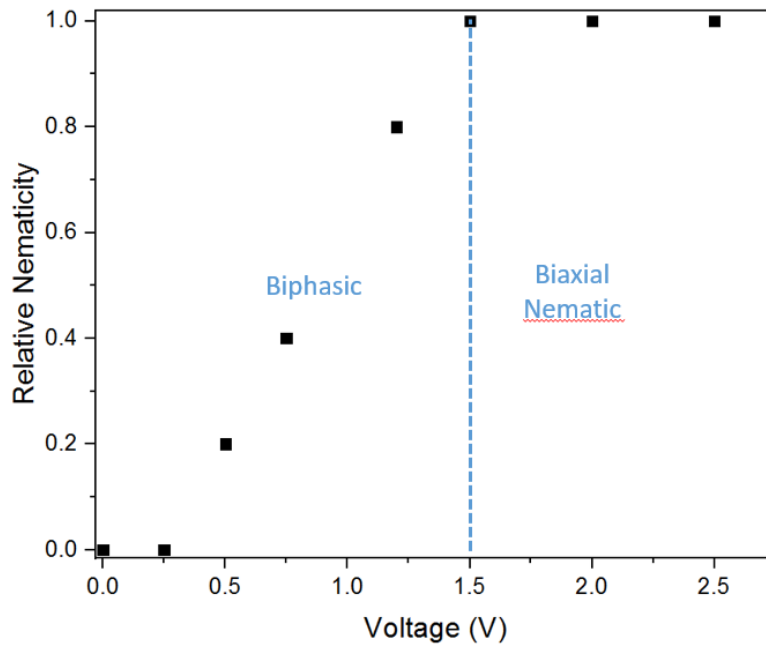


Figure 23. Schlieren Texture of particles at a) 0V, b) 0.5V, c) 0.75V, d) 1.25V, e) 1.5V, f) 1.5V for $\phi = 0.012 \pm 0.001$. Observed texture changes are applicable to $\phi_i < \phi < \phi_N$. Application of the electric field induces brightening as well as a uniaxial-biaxial transition. The uniaxial defects are characterized by four dark brushes while the biaxial defects are characterized by two dark brushes.

The transition point to be defined is that from the uniaxial-biaxial coexistence region to the wholly biaxial region. This is the point where all uniaxial defects ($s=1$) are split into biaxial defects ($s = \frac{1}{2}$). Polarized images in figure 23 above were characterized on Image J; the relative area occupied by uniaxial vs biaxial defects was quantified. A linear extrapolation, as in figure 24 below, was made to the point of 0% uniaxial defects and this yielded an applied voltage of 1.4V. This is defined as the transition point for volume fraction $\phi = 0.012$.

Figure 24. First Order Transition Voltage Extrapolation $\phi = 0.012 \pm 0.001$. The transition voltage is defined as 1.5V



(0.0117V/ μm). This represents the transition from the coexistence to the biaxial region.

This procedure was repeated for volume fractions of 0.011 and 0.010 to yield transition voltages of 2.5V and 4.5V respectively. The table below summarizes the transition voltages defined

Volume Fraction (ϕ)	Transition Voltage (V)
0.010	4.5 ± 0.5
0.011	2.5 ± 0.3
0.012	1.5 ± 0.2

Table 4. Transition voltages for samples within volume fraction ($\phi_I < \phi < \phi_N$). The transition point decreases roughly linearly with volume fraction.

To further prove the transition from uniaxial to biaxial phase, magnified observations of the splitting of defects was recorded for volume fraction $\phi = 0.011$. As can be observed below, the biaxial phase is composed of $S = \frac{1}{2}$ defects with two dark brushes. These were experimentally observed to form as a result of the splitting of the uniaxial $S=1$ defects with four dark brushes. The splitting occurred over the order of a few minutes.

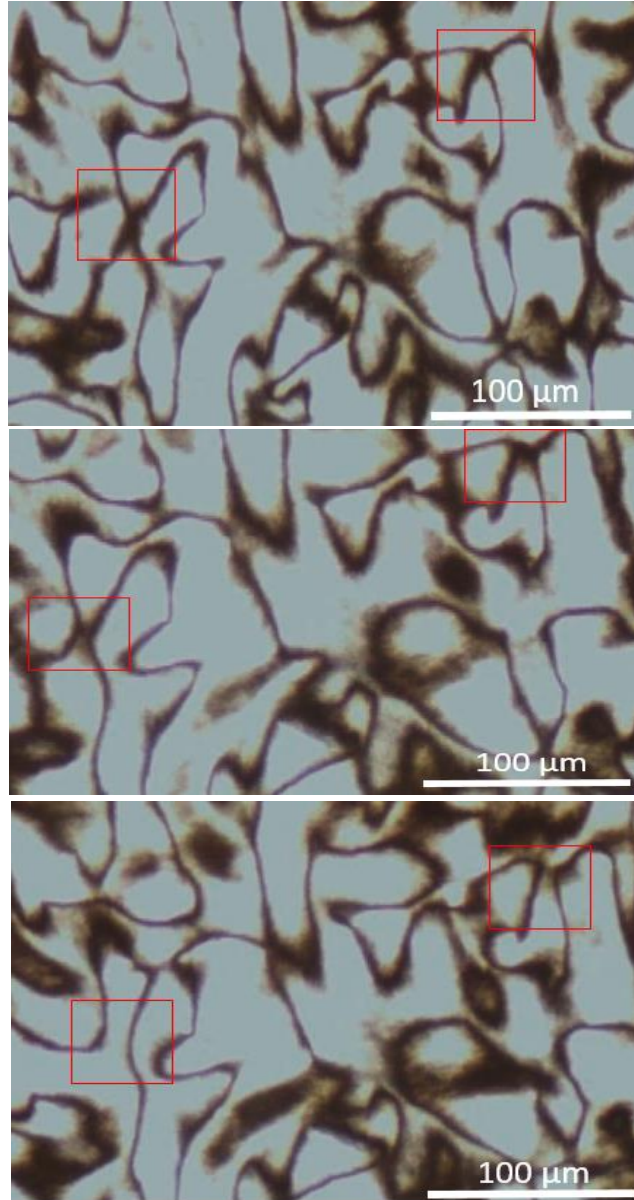


Figure 25. Defect Splitting in the Nematic Phase for $\phi = 0.011 \pm 0.001$ with applied voltage of $2.5V_{pp}$. The biaxial nematic phase is featured with two dark brushes, which are formed by the splitting of four dark brushes. The red boxes indicate the splitting points. Figure (a) was taken at 0 minutes; (b) after 10 minutes; (c) after 25 minutes.

Second Order Transition ($\phi < \phi_c$)

The tricritical point ϕ_c was deduced as the point of convergence of both transition lines as in I and II above. Thereafter, electric field was applied to samples with volume fraction less than the tricritical volume fraction ϕ_c . The schematic for the experimentation is below

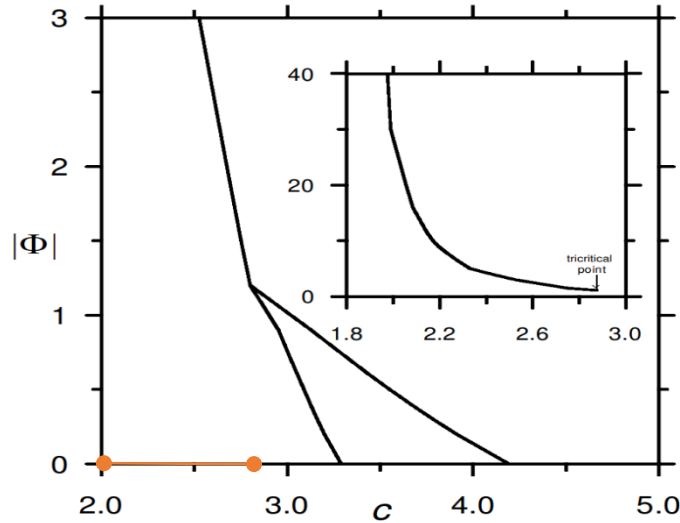


Figure 26. Schematic for experimentation to determine second order transition points for ZrP platelets in volume fraction ranges ($\phi < \phi_c$) within the electric field.

Experiments were aimed at observing the paranematic-biaxial transition in such particles. The polarized microscopic textures depicted below indicates second order transition from the isotropic to the biaxial nematic phase. Figures below relate to voltages applied for volume fraction $\phi = 0.0032$. The texture remains dark up until the application of 300 V; where biaxial defects spontaneously form without crystal formation and growth. This is defined as the transition voltage.

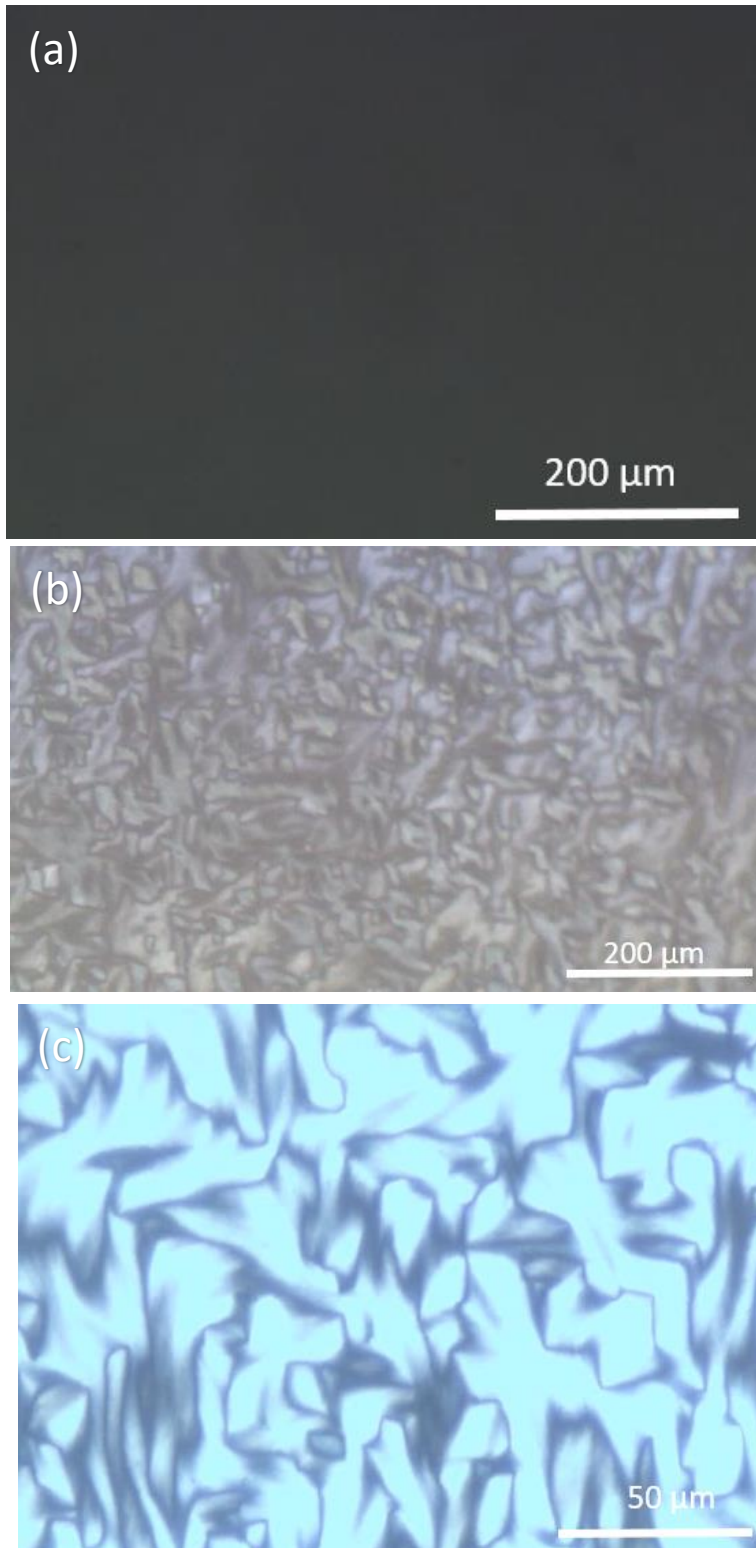


Figure 27. Microscopic enlargement of particles at a) 250V, b) 300V, c) 300V for $\phi = 0.0032 \pm 0.0002$. Observed texture changes is applicable to $\phi < \phi_c$. Application of electric field below this concentration leads to a second order transition to the biaxial phase.

This procedure was repeated for volume fractions 0.0025 and 0.0020 to yield transition voltages of 350 V and 500 V respectively.

Volume Fraction (ϕ)	Transition Voltage (V)
0.0020	500 \pm 50
0.0025	350 \pm 35
0.0032	300 \pm 30

Table 5. Transition voltages for samples within volume fraction ($\phi_l < \phi < \phi_N$). The transition point decreases exponentially with volume fraction.

Phase Diagram

Pertinent to previous investigations, the phase diagram was constructed in an electric field parameter - reduced concentration plane. The electric field parameter (Φ) is described by the equation $\Phi = \frac{\Delta\alpha E^2}{4kT}$. Where E represents the field strength in units of voltage peak-to-peak (V_{pp}) per length, k represents the Boltzmann constant and $\Delta\alpha$ represents the anisotropy estimated to the order of 10^{-29} based on previous birefringence spectroscopy correlations for Zirconium Phosphate nanoparticles by Shinde et al. The reduced concentration is given by $c = \frac{\pi^2 D^3 N}{16V}$; where D represents the diameter of particles, N represent the number of particles and V represents the volume of a single particle.

Drawing upon transition voltages collected, a full phase diagram was implemented as below:

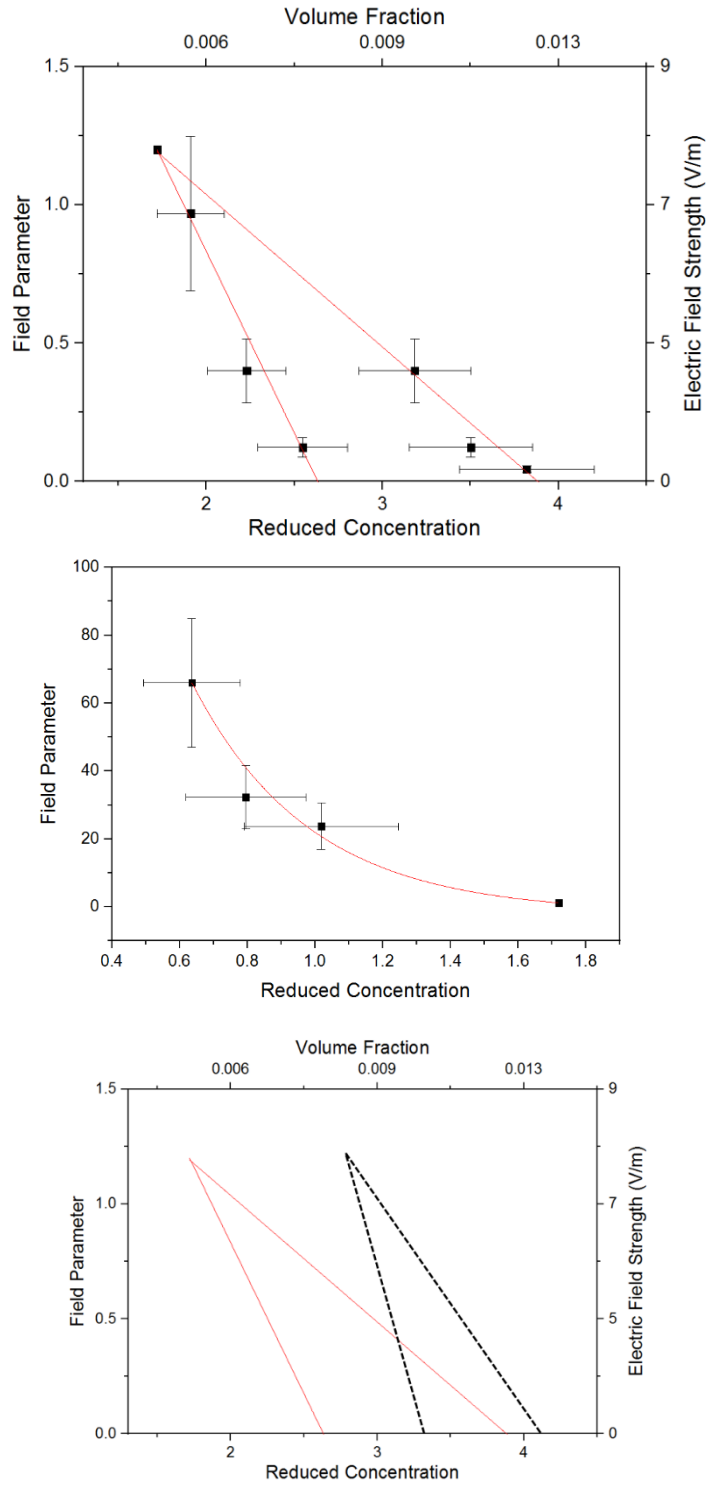


Figure 28. Phase diagram of a) first order transition b) second order transition c) comparison of first order transition to Varga's simulation, for ZrP particles under the effects of an electric field.

The tricritical point for ZrP platelets occurred at a reduced concentration of 1.7. The biphasic region for our system occurs at lower concentrations due to the inherent polydispersity of the platelets. At the tri-critical point, a first order transition halted and was replaced with a second order transition. Previous simulations by Varga et al yielded the tricritical point at a reduced concentration of 2.8 and an electric field parameter of 1.2, while Khoklov and Semenov's work yielded the tricritical point at a reduced concentration of 2.4 and an electric field parameter of 2.2. These differences could be explained by the crude approximations underlying in the trial functions employed.

CHAPTER V: CONCLUSIONS AND FUTURE WORK

These studies focused on the phase transitions of negatively anisotropic discotic liquid crystals in the presence of external fields. Zirconium phosphate disks were synthesized by hydrothermal method and diluted to very low volume fractions with range 0.006 to 0.015. We observed an isotropic-nematic transition with increasing concentration of the platelets, as predicted by Onsager's theory. For increasing volume fraction of the disks, the nematic fraction within the solution increased.

Schlieren textures depicting discontinuity and defects in the orientation of the nanoplates were analyzed between cross polarizers in a microscope. The textures of the nematic phase was observed before and after application of an electric field ($\theta_\phi = 0$). At a constant field strength of 0.025 V/m, we demonstrated that smaller spacer thicknesses provided clearer textures of the nematic liquid crystal defects. As the cell thickness and sample volume increased schlieren textures became increasingly distorted.

Electric field induced alignment of these negatively dielectric disks yielded the occurrence of a first order transition which entailed a biphasic region between the uniaxial nematic and biaxial nematic phase. This first-order transition is characterized by the increase in brightness of the schlieren texture and formation of crystals, and it converges with a second order transition at a tricritical point. The phase diagram constructed is qualitatively in line with theoretical extensions of Onsager's theory for isotropic-nematic transition.

The results from these experiments yielded for the first time experimentally, to the best of our knowledge, the demonstration of the biaxial nematic phase in negatively anisotropic

discotic liquid crystals. This higher-order nematic phase poses potential for application in 3D imaging as a result of the ability to control alignment across two particulate axes with the one-directional application of electric field. Future experimentations could include an investigation of nature of particle interactions at the tricritical point. Furthermore, the kinetics of disclination splitting / rotation, and defect density variation with electric field intensity should be explored.

REFERENCES

- 1 O'Neill, Mary, and Stephen M. Kelly. "Ordered materials for organic electronics and photonics." *Advanced Materials* 23.5 (2011): 566-584.
- 2 Jones, Richard AL. *Soft condensed matter*. Vol. 6. Oxford University Press, 2002.
- 3 Beek, David van der. *Liquid crystal phase behaviour of colloidal platelets in external fields*. Utrecht University, 2005.
- 4 Komitov, Lachezar. "Molecular Shape Related Effects in Liquid Crystals." *Molecular Crystals and Liquid Crystals* 608.1 (2015): 246-257.
- 5 Onsager, Lars. "The effects of shape on the interaction of colloidal particles." *Annals of the New York Academy of Sciences* 51.4 (1949): 627-659.
- 6 Tschierske, Carsten, and Demetri J. Photinos. "Biaxial nematic phases." *Journal of Materials Chemistry* 20.21 (2010): 4263-4294. S. Varga, K. Gergely, and S. Istvan, *Molecular Physics*, **98**, 2000, 911-915.
- 7 Van den Pol, E., et al. "Uniaxial and biaxial liquid crystal phases in colloidal dispersions of board-like particles." *Liquid Crystals* 37.6-7 (2010): 641-651.
- 8 De Oliveira, B. F., et al. "Nematic liquid crystal dynamics under applied electric fields." *Physical Review E* 82.4 (2010): 041707.
- 9 Lee, Ji-Hoon, et al. "Dynamics of electro-optical switching processes in surface stabilized biaxial nematic phase found in bent-core liquid crystal." *Journal of applied physics* 101.3 (2007): 034105.
- 10 Reinink, ABGM Leferink, et al. "Phase behaviour of lyotropic liquid crystals in external fields and confinement." *The European Physical Journal Special Topics* 222.11 (2013): 3053-3069.

- 11 Khokhlov, A. R., and A. N. Semenov. "Influence of external field on the liquid-crystalline ordering in the solutions of stiff-chain macromolecules." *Macromolecules* 15.5 (1982): 1272-1277.
- 12 Szalai, Szabolcs et al. "External field induced paranematic–nematic phase transitions in rod-like systems." *Molecular Physics* 93.3 (1998): 377-387.
- 13 Chiccoli, C., et al. "Topological defects in schlieren textures of biaxial and uniaxial nematics." *Physical Review E* 66.3 (2002): 030701.
- 14 Chen, Mingfeng, et al. "Rainbows in a vial: controlled assembly of 2D colloids in two perpendicular external fields." *2D Materials* 6.2 (2019): 025031.
- 15 Van der Kooij, Felix M., Katerina Kassapidou, and Henk NW Lekkerkerker. "Liquid crystal phase transitions in suspensions of polydisperse plate-like particles." *Nature* 406.6798 (2000): 868.[13]
- 16 Eppenga, R., and Daan Frenkel. "Monte Carlo study of the isotropic and nematic phases of infinitely thin hard platelets." *Molecular physics* 52.6 (1984): 1303-1334.
- 17 Parsons, J. D. "Nematic ordering in a system of rods." *Physical Review A* 19.3 (1979): 1225.
- 18 Van der Beek, D., et al. "Magnetic-field-induced orientational order in the isotropic phase of hard colloidal platelets." *Physical Review E* 73.4 (2006): 041402.
- 19 Van der Beek, D., et al. "Influence of a magnetic field on the nematic phase of hard colloidal platelets." *Physical Review E* 77.3 (2008): 031708.
- 20 Mejia, Andres F., et al. "Aspect ratio and polydispersity dependence of isotropic-nematic transition in discotic suspensions." *Physical Review E* 85.6 (2012): 061708.

- 21 Shinde, Abhijeet, Xuezheng Wang, and Zhengdong Cheng. "Aspect Ratio Dependence of Isotropic-Nematic Phase Separation of Nanoplates in Gravity." *Gravitational and Space Research* 4.1 (2016).
- 22 Shuai, Min, et al. "Hydrothermal synthesis of layered α -zirconium phosphate disks: control of aspect ratio and polydispersity for nano-architecture." *CrystEngComm* 15.10 (2013): 1970-1977. [20]
- 23 Lagerwall, Jan PF, and Giusy Scalia. "A new era for liquid crystal research: Applications of liquid crystals in soft matter nano-, bio-and microtechnology." *Current Applied Physics* 12.6 (2012): 1387-1412. (various molecules form various phases of LC)
- 24 Sluckin, Timothy J., David A. Dunmur, and Horst Stegemeyer. *Crystals that flow: classic papers from the history of liquid crystals*. CRC Press, 2004.
- 25 Bisoyi, Hari Krishna, and Sandeep Kumar. "Liquid-crystal nanoscience: an emerging avenue of soft self-assembly." *Chemical Society Reviews* 40.1 (2011): 306-319. LC important in self assembly
- 26 Hällstig, Emil. *Nematic liquid crystal spatial light modulators for laser beam steering*. Diss. Acta Universitatis Upsaliensis, 2004.
- 27 "Nature's Liquid Crystals." *CNRS News*, 2018, [news.cnrs.fr/articles/natures-liquid-crystals](https://www.cnrs.fr/articles/natures-liquid-crystals).
- 28 Guo, Chenyu, et al. "Lyotropic liquid crystal systems in drug delivery." *Drug discovery today* 15.23-24 (2010): 1032-1040.
- 29 Kasch, Nicholas. "Liquid crystals: applications and industry." (2013): 19-20. (LC in drug delivery)
- 30 "How Does Kevlar Work?: Why Is Kevlar so Strong?" *Explain That Stuff*, 12 July 2019, www.explainthatstuff.com/kevlar.html.

- 31 "Liquid Crystal Displays." *Lecture 1 --- 6.837 Fall '01*, 2001, groups.csail.mit.edu/graphics/classes/6.837/F01/Lecture01/Slide16.html.
- 32 Shibaev, Valery P., and Alexey Yu Bobrovsky. "Liquid crystalline polymers: development trends and photocontrollable materials." *Russ. Chem. Rev* 86.11 (2017): 1024-1072.
- 33 "Textures of Liquid Crystals." *Liquid Crystals: a Simple View on a Complex Matter*, 1992, www.personal.kent.edu/~bisenyuk/liquidcrystals/textures1.html.
- 34 "High Strength Defects in Nematic Liquid Crystals." *Raman Research Institute*, 2011, dspace.rrri.res.in/bitstream/2289/3502/11/Chapter%206.pdf.
- 35 Sherrill, David. "The Variational Method." *The Variational Method*, 2006, vergil.chemistry.gatech.edu/notes/quantrev/node28.html.
- 36 Franco-Melgar, Mario, Andrew J. Haslam, and George Jackson. "A generalisation of the Onsager trial-function approach: describing nematic liquid crystals with an algebraic equation of state." *Molecular Physics* 106.5 (2008): 649-678. indepth on onsagers theory
- 37 Meija, Carlos. "Electric Field Induced Birefringence in Isotropic Suspensions of Nanoplates", 2017.
- 38 A. AlSunaidi, W. K. den Otter, J. H. R. Clarke. Inducement by directional fields of rotational and translational phase ordering in polymer liquid-crystals. *The Journal of Chemical Physics* **2013**, 138 (15) , 154904. DOI: 10.1063/1.4798462.
- 39 Akihiko Matsuyama. Biaxial nematic phases in rod/liquid crystal mixtures. *Liquid Crystals* **2011**, 38 (6) , 729-736. DOI: 10.1080/02678292.2011.570795.
- 40 H. H. Wensink, G. J. Vroege. Nematic order of model goethite nanorods in a magnetic field. *Physical Review E* **2005**, 72 (3) DOI: 10.1103/PhysRevE.72.031708.

- 41 David C. Williamson, Neil A. Thacker, Stephen R. Williams. Effects of intramolecular dipolar coupling on the isotropic-nematic phase transition of a hard spherocylinder fluid. *Physical Review E* **2005**, 71 (2) DOI: 10.1103/PhysRevE.71.021702.
- 42 P. Teixeira, M. Osipov, M. Telo da Gama. Phase diagrams of aligned dipolar hard rods. *Physical Review E* **1998**, 57 (2) , 1752-1760. DOI: 10.1103/PhysRevE.57.1752.
- 43 Seth Fraden. Phase Transitions in Colloidal Suspensions of Virus Particles. **1995**, 113-164. DOI: 10.1007/978-94-011-0065-6_3.
- 44 Reichenstein, M., et al. "Motion, creation, and annihilation of disclinations in multidomain structured nematic liquid crystal cells." *Physical Review E* 65.1 (2001): 011709.
- 45 Ostapenko, T., et al. "Magnetic-field induced isotropic to nematic liquid crystal phase transition." *Physical review letters* 101.24 (2008): 247801.
- 46 Chandrasekhar, S., and G. S. Ranganath. "The structure and energetics of defects in liquid crystals." *Advances in Physics* 35.6 (1986): 507-596.
- 47 Priezjev, Nikolai V., and Robert A. Pelcovits. "Coarsening dynamics of biaxial nematic liquid crystals." *Physical Review E* 66.5 (2002): 051705.
- 48 Lingyu Luan, Wei Li, Shangying Liu and Dejun Sun. Phase Behavior of Mixtures of Positively Charged Colloidal Platelets and Nonadsorbing Polymer. *Langmuir* **2009**, 25 (11) , 6349-6356. DOI: 10.1021/la804023b
- 49 G. Viau,, R. Brayner,, L. Poul,, N. Chakroune,, E. Lacaze,, F. Fiévet-Vincent, and, F. Fiévet. Ruthenium Nanoparticles: Size, Shape, and Self-Assemblies. *Chemistry of Materials* **2003**, 15 (2), 486-494. DOI: 10.1021/cm0212109.
- 50 Laurent J. Michot,, Isabelle Bihannic,, Katharina Porsch,, Solange Maddi,, Christophe Baravian,, Julien Mougel, and, Pierre Levitz. Phase Diagrams of

- Wyoming Na-Montmorillonite Clay. Influence of Particle Anisotropy. *Langmuir* **2004**, *20* (25) , 10829-10837. DOI: 10.1021/la0489108
- 51 Vivek Sharma, Kyoungweon Park, Mohan Srinivasarao. Colloidal dispersion of gold nanorods: Historical background, optical properties, seed-mediated synthesis, shape separation and self-assembly. *Materials Science and Engineering: R: Reports* **2009**, *65* (1-3) , 1-38. DOI: 10.1016/j.mser.2009.02.002.
- 52 Z. X. Zhang, Jeroen S. van Duijneveldt. Isotropic-nematic phase transition of nonaqueous suspensions of natural clay rods. *The Journal of Chemical Physics* **2006**, *124* (15) , 154910. DOI: 10.1063/1.2185642.
- 53 A. S. Sonin, N. A. Churochkina, A. V. Kaznacheev, A. V. Golovanov. Mineral liquid crystals. *Colloid Journal* **2017**, *79* (4) , 421-450. DOI: 10.1134/S1061933X17040159.
- 54 Xi Lin, Dirk Schmelter, Sadaf Imanian, Horst Hintze-Bruening. Hierarchically Ordered α -Zirconium Phosphate Platelets in Aqueous Phase with Empty Liquid. *Scientific Reports* **2019**, *9* (1) DOI: 10.1038/s41598-019-51934-y.
- 55 Jize Sui, Yiming Ding, Masao Doi. Dynamics of liquid crystalline phase transition in sedimenting platelet-like particles. *Soft Matter* **2018**, *14* (16) , 3049-3056. DOI: 10.1039/C8SM00254A.
- 56 Rachel Tkacz, Md Joynul Abedin, Phillip Sheath, Shalin B. Mehta, Amitabh Verma, Rudolf Oldenbourg, Mainak Majumder. Phase Transition and Liquid Crystalline Organization of Colloidal Graphene Oxide as a Function of pH. *Particle & Particle Systems Characterization* **2017**, *34* (9) , 1600391. DOI: 10.1002/ppsc.201600391.
- 57 Huawei Li, Xuezhen Wang, Ying Chen, Zhengdong Cheng. Temperature-dependent isotropic-to-nematic transition of charged nanoplates. *Physical Review E* **2014**, *90* (2) DOI: 10.1103/PhysRevE.90.020504.

- 58 Liang Wu, George Jackson, Erich Müller. Liquid Crystal Phase Behaviour of Attractive Disc-Like Particles. *International Journal of Molecular Sciences* **2013**, *14* (8) , 16414-16442. DOI: 10.3390/ijms140816414.
- 59 L. Harnau. Structure and thermodynamics of platelet dispersions. *Molecular Physics* **2008**, *106* (16-18) , 1975-2000. DOI: 10.1080/00268970802032301.
- 60 E. P. Sokolova, N. P. Tumanyan, A. YU. Vlasov, A. J. Masters. Zwanzig model of multi-component mixtures of biaxial particles: γ_3 theory re-visited. *Molecular Physics* **2006**, *104* (18) , 2901-2917. DOI: 10.1080/00268970600867429.
- 61 H. H. Wensink, G. J. Vroege. Phase equilibria in systems of hard disks with thickness polydispersity. *Physical Review E* **2002**, *65* (3) DOI: 10.1103/PhysRevE.65.031716.
- 62 Liu Y, Xu Z, Gao W, Cheng Z and Gao C 2017 Graphene and other 2D colloids: liquid crystals and macroscopic fibers *Adv. Mater.* **29** 1606794
- 63 Jiménez M L, Fornasari L, Mantegazza F, Mourad M C D and Bellini T 2012 Electric birefringence of dispersions of platelets
- 64 Shen, Tian-Zi, Seung-Ho Hong, and Jang-Kun Song. "Electro-optical switching of graphene oxide liquid crystals with an extremely large Kerr coefficient." *Nature materials* *13.4* (2014): 394-399.
- 65 O'Neill, Mary, and Stephen M. Kelly. "Liquid crystals for organic field-effect transistors." *Liquid Crystalline Semiconductors*. Springer, Dordrecht, 2013. 247-268.
- 66 O'Neill M and Kelly S M 2011 Ordered materials for organic electronics and photonics *Adv. Mater.* **23** 566
- 67 Bragg W L and Pippard A B 1953 The form birefringence of macromolecules *Acta Cryst.* **6** 865

- 68 Sui J, Ding Y and Doi M 2018 Dynamics of liquid crystalline phase transition in sedimenting platelet-like particles *Soft Matter* **14** 3049
- 69 Clearfield A and Stynes J 1964 The preparation of crystalline zirconium phosphate and some observations on its ion exchange behaviour *J. Inorg. Nucl. Chem.* **26** 11
- 70 "What Is the Boltzmann Constant." *Boltzmann Constant*, 2018, www.calculator.org/properties/Boltzmann_constant.html. **what is N**
- 71 Bhagat, Bhushan. "What Is LCD DISPLAY?" *Explain Liquid Crystal*, 1 Jan. 1970, newtechnicalbuddy.blogspot.com/2016/11/what-is-lcd-display-explain-liquid.html.
- 72 Varga, Szabolcs, Gergely Kronome, and Istvan Szalai. "External field induced tricritical phenomenon in the isotropicnematic phase transition of hard non-spherical particle systems." *Molecular Physics* 98.14 (2000): 911-915.